Determination of Absolute Configuration and Conformation of a Cyclic Dipeptide by NMR and Chiral Spectroscopic Methods

ARTICLE *in* THE JOURNAL OF PHYSICAL CHEMISTRY A · JANUARY 2013

Impact Factor: 2.69 · DOI: 10.1021/jp311151h · Source: PubMed

11 AUTHORS, INCLUDING:

Jana Novotná
University of Chemistry and Technology, Prague
10 PUBLICATIONS **102** CITATIONS
SEE PROFILE

Wenche Stensen
University of Tromsoe
27 PUBLICATIONS **794** CITATIONS
SEE PROFILE

Valery Andrushchenko
Academy of Sciences of the Czech Republic
56 PUBLICATIONS **899** CITATIONS
SEE PROFILE

John Sigurd Svendsen
University of Tromsoe
92 PUBLICATIONS **2,937** CITATIONS
SEE PROFILE

THE JOURNAL OF PHYSICAL CHEMISTRY A

Article

pubs.acs.org/JPCA

Determination of Absolute Configuration and Conformation of a Cyclic Dipeptide by NMR and Chiral Spectroscopic Methods

Xiaojun Li,[†] Kathrin H. Hopmann,*[,†,‡] Jana Hudecová,[§] Johan Isaksson,[‡] Jana Novotná,[∥] Wenche Stensen,[⊥] Valery Andrushchenko,[§] Marie Urbanová,[#] John-Sigurd Svendsen,[‡] Petr Bouř,*[,§] and Kenneth Ruud[†]

[†]Centre for Theoretical and Computational Chemistry (CTCC) and [‡]Department of Chemistry, University of Tromsø, N-9037 Tromsø, Norway

[§]Institute of Organic Chemistry and Biochemistry, Academy of Sciences, Prague, 166 10 Prague, Czech Republic

[∥]Department of Analytical Chemistry and [#]Department of Physics and Measurements, Institute of Chemical Technology, Prague, 166 28 Prague, Czech Republic

[⊥]Lytix Biopharma AS, Tromsø Research Park, N-9294 Tromsø, Norway

Supporting Information

ABSTRACT: Increasing precision of contemporary computational methods makes spectroscopies such as vibrational (VCD) and electronic (ECD) circular dichroism attractive for determination of absolute configurations (AC) of organic compounds. This is, however, difficult for polar, flexible molecules with multiple chiral centers. Typically, a combination of several methods provides the best picture of molecular behavior. As a test case, all possible stereoisomers with known AC (*RS*, *SR*, *SS*, and *RR*) of the cyclic dipeptide cyclo(Arg-Trp) (CAT) were synthesized, and the performances of the ECD, infrared (IR), VCD, Raman, Raman optical activity (ROA), and nuclear magnetic resonance (NMR) techniques for AC determination were investigated. The spectra were interpreted with the aid of density functional theory (DFT) calculations. Folded geometries stabilized by van der Waals and electrostatic interactions between the diketopiperazine (DKP) ring and the indole group are predicted to be preferred for CAT, with more pronounced folding due to Arg-Trp stacking in the case of *SS*/*RR*-CAT. The *RS*/*SR* isomers prefer a twist-boat puckering of the DKP ring, which is relatively independent of the orientation of the side chains. Calculated conformer-averaged VCD and ECD spectra explain most of the experimentally observed bands and allow for AC determination of the tryptophan side-chain, whereas the stereochemical configuration of the arginine side-chain is visible only in VCD. NMR studies provide characteristic long-range ^{2}J(C,H) and ^{3}J(C,H) coupling constants, and nuclear Overhauser effect (NOE) correlations, which in combination with either ECD or VCD also allow for complete AC determination of CAT.

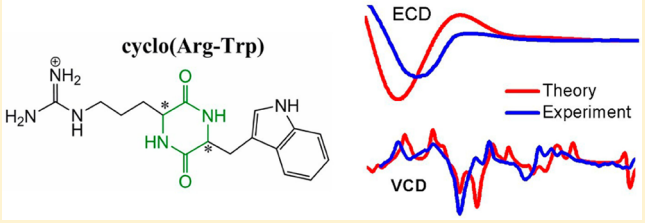

INTRODUCTION

Cyclic dipeptides are an important class of biomolecules with multifunctional groups. Since the crystal structure of 2,5-Diketopiperazines (DKPs) was first observed by R. B. Corey in 1938,[1] DKP derivatives have attracted significant attention because of their potential use in many pharmacological applications, for example, as antibacterial,[2,3] antitumor,[4,5] anticancer,[6] and antiviral[7] agents. Other important biological activities associated with DKPs are in the alteration of cardiovascular and blood-clotting functions,[8] and their affinities to a variety of receptors.[9−12] Several DKP derivatives are found to be of interest as effective chitinase inhibitors by structurally mimicking a reaction intermediate,[13] as well as being ideal compounds for the rational design of new drugs.[14]

The molecular recognition and thermodynamic properties of DKP derivatives are expected to be useful for understanding protein folding.[15,16] For example, the absolute configuration (AC) of the compounds determines their supramolecular structure. Different enantiomeric forms create different macromolecular self-assemblies, e.g., due to differences in intra- and intermolecular hydrogen bonding.[17] Investigations of the conformational and electronic properties of DKPs are thus valuable also for an understanding of their biological activity.

Computer-aided investigations provide insight into the link between the energetic, structural, and spectroscopic properties of molecules.[18−24] A recent review by Cohen et al.[25] summarizes some of the successes and challenges of density functional theory (DFT) in this area. For example, to obtain reliable results, one has to overcome the inability of some functionals to describe the attractive long-range van der Waals interactions, which are essential for molecular folding. A very efficient method to address this shortcoming of DFT has been

Received: November 11, 2012
Revised: January 24, 2013
Published: January 24, 2013

dx.doi.org/10.1021/jp311151h | *J. Phys. Chem. A* 2013, 117, 1721−1736

the empirical dispersion correction introduced by Grimme, lately further extended over the entire periodic table and different bonding situations.[26−28] This "DFT-D" approach provides results with an accuracy comparable to that of some correlated wave function methods, such as MP2.[29−31]

Low-resolution conformationally oriented spectroscopies are essential tools to monitor molecules in solutions. Several spectroscopic studies of cyclic dipeptides have been presented in the past, using for instance infrared absorption (IR) and Raman,[32−36] nuclear magnetic resonance (NMR),[37−42] vibrational circular dichroism (VCD) and Raman optical activity (ROA),[29] ultraviolet (UV) absorption,[43,44] and electronic circular dichroism (ECD).[44−46]

Vibrational optical activity (VOA) is particularly useful for AC determinations. VCD[47,48] and ROA[23,49−52] techniques are based on the differential infrared absorption and Raman scattering of the left- and right-circularly polarized light, respectively. VOA usually exploits the vibrational transitions within the electronic ground state. It is rather sensitive to the mutual orientation of distinct groups in the molecule, thus providing valuable three-dimensional structural information for determination of the absolute configuration. VCD and ROA have been widely applied to determine the ACs of chiral structures of small molecules,[40,53−55] as well as to structural studies of proteins,[20,56,57] viruses,[58,59] and drugs.[60,61] The two techniques have also been successfully used for the determination of the ACs of chiral molecules with multiple stereocenters,[29,40,61−63] although cases have been reported in which, e.g., VCD has failed to resolve the configuration of all stereocenters.[64]

Electronic-excitations based optical rotation[65,66] (OR) and electronic circular dichroism[66,67] (ECD) are also often employed in AC assignments. The availability of reasonably fast and accurate time-dependent DFT (TD-DFT) methods boosted the reliability of these approaches.[65,68,69] Ordinary ORD or ECD spectra, however, exhibit a limited number of features,[67] making comparison to theory difficult due to the challenges in obtaining reliable theoretical ORD and ECD data. These techniques are also very sensitive to solvent and temperature variations.[70,71]

NMR spectroscopy can also be applied in the determination of stereochemistry as many NMR-derived parameters are tightly bound to the conformation. These range from the traditional chemical shifts, homo- and heteronuclear coupling constants and NOE-derived distance restraints to more recently explored residual dipolar couplings (RDCs) and residual chemical shift anisotropy (RCSA) of partially aligned molecules in liquid crystalline media or stretch gels developed for small organic molecules.[72−75] As conventional NMR is blind to chirality, NMR AC determinations have been limited to product analysis after chemical derivatization with a chiral agent or analysis of a complex with chiral solvents or chiral metal complexes.[76] At least theoretically, AC can be determined from RDCs measured in nonracemic chiral liquid crystalline solvents or gel polymers.[77,78] These methods, however, depend on accurate predictions of the diastereomorphous conformations formed upon interactions with the chiral environment, or possibly on the analysis of a series of closely related compounds, an approach that does not seem feasible with available technologies so far. The reliability and validity of some AC determinations in chiral alignment media have been questioned very recently.[79]

In this work, we investigate how the known AC of protonated cyclo(Arg-Trp) (CAT) is reflected in the IR/VCD, Raman/ROA, ECD, and NMR parameters of its different stereoisomers, and how the spectral and conformational properties of CAT can be retrieved from computations. The CAT molecule has two stereocenters (C_1 and C_4, Figure 1),

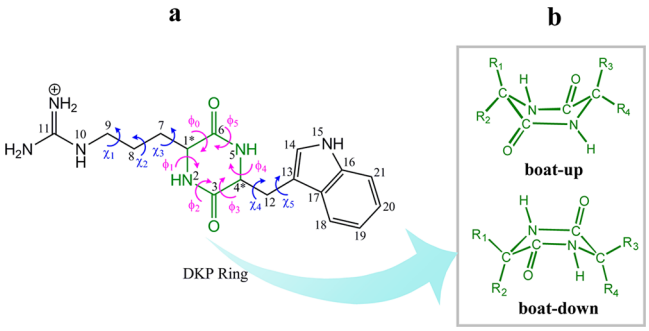

Figure 1. (a) Protonated cyclo(Arg-Trp) (CAT) with atom labeling (arbitrary) and definition of the main torsion angles used in the analysis of the structural flexibility. The two chiral centers (C_1 and C_4) are labeled with asterisks. (b) Two possible conformations of the DKP ring: boat-up and boat-down (R1, R2 = H and Arg side chain, R3, R4 = H and Trp side chain).

resulting in four stereoisomers (*RS*, *SR*, *SS*, and *RR*, where e.g., *RS* = 1*R*,4*S*). The computational study shows that the conformer stability for the different isomers is strongly dependent on the description of nonbonded interactions, e.g., the dispersion forces between aliphatic and aromatic parts ("C−H···π") and hydrogen bonds. The arginine side chain of CAT has a high degree of flexibility, requiring optimization of different conformers and averaging of theoretical spectra to obtain reliable results. The experimental and theoretical VCD, Raman, ECD, and NMR parameters provide useful information about the stereochemical and conformational properties of CAT. A full AC assignment of CAT is possible with VCD only, or with a combination of ECD and NMR methods.

RESULTS AND DISCUSSION

Structural Analysis. The four stereoisomers of CAT (*RS*, *SR*, *SS*, and *RR*) were optimized at the B3LYP-D/6-31++G**/IEFPCM(methanol) level of theory. Because the *RS* and *SR* as well as *SS* and *RR* isomers are mirror images of each other, only the *RS*- and *SS*-CAT conformers are presented in Figures 2 and 3, respectively.

In the *RS*-CAT conformers, the arginine and tryptophan side chains are located "above" and "below" the DKP ring, respectively. The inclusion of empirical dispersion corrections in the geometry optimizations leads to formation of C_αH···π intramolecular interactions between the DKP ring and the indole group, resulting in folded conformations, as also found in an earlier study of similar cyclic dipeptides.[80] As can be seen from Table 1 (and Figure 2), the folded structures a1−a4 are stabilized by C_αH···π and NH···O intramolecular interactions with distances of 2.446−2.572 and 1.753−1.789 Å, respectively; the a5 conformer results from C_αH···π and C_δH···π attractions, with distances of 2.446 and 2.614 Å, respectively.

The orientation of the indole group with respect to the arginine side chain affects the structural stability slightly; conformers with the indole ring and the guanidinium side chains pointing to opposite sides (conformers a1 and a3) are

dx.doi.org/10.1021/jp311151h | J. Phys. Chem. A 2013, 117, 1721−1736

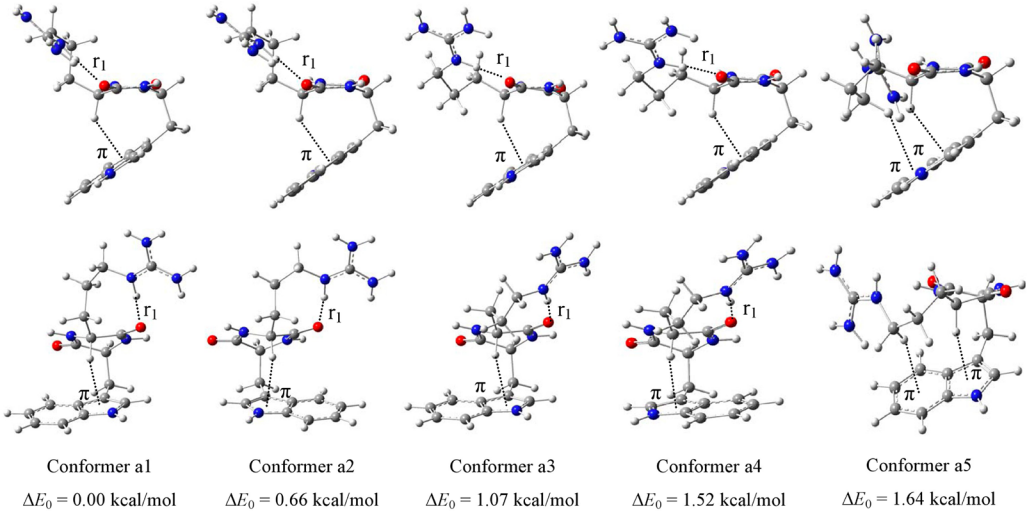

Figure 2. Optimized structures of the five most stable *RS* conformers of protonated CAT, obtained at the B3LYP-D/6-31++G**/IEFPCM(methanol) level of theory. Each conformer is shown as a front and side view, relative energies include zero-point vibrational correction.

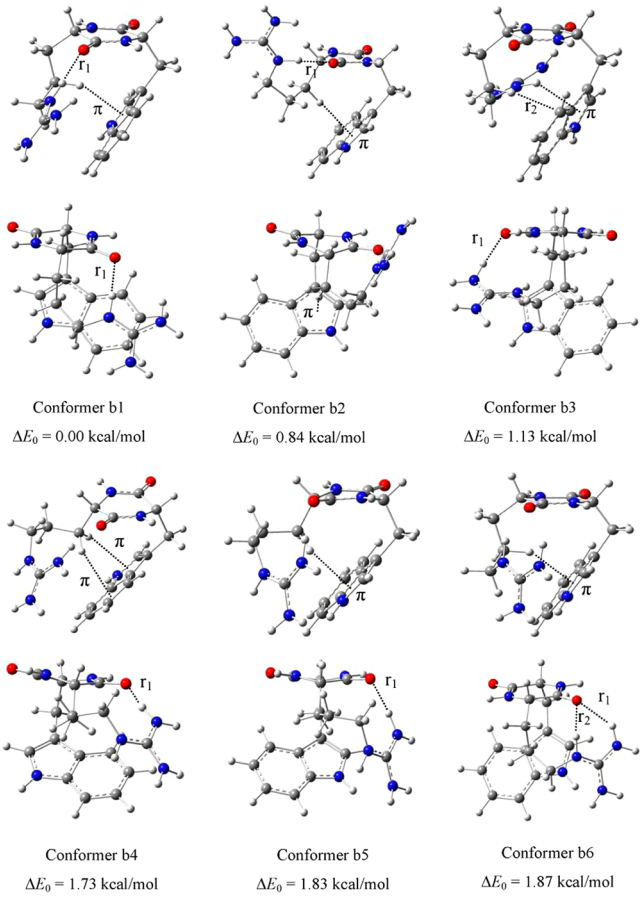

Figure 3. Optimized structures of the six most stable *SS* conformers of protonated CAT, obtained at the B3LYP-D/6-31++G**/IEFPCM-(methanol) level of theory.

~0.5 kcal/mol lower in energy than corresponding conformers with the indole ring and guanidinium pointing to the same side (conformers a2 and a4, Figure 2). The folding of the arginine side chain relative to the DKP ring affects the relative energies more significantly; conformers where the arginine chain folds upward (a1 and a2, with N−C_α−C_β−C_γ angle of ~−64°) are by ~1 kcal/mol lower in energy than conformers where the arginine folds sideways (a3 and a4 with N−C_α−C_β−C_γ angle of 155°). Structures with a boat-up DKP conformation are less stable (<2%). The zero-point vibrational energy (ZPVE) influences the relative stability and thus has to be taken into account when the Boltzmann populations are determined (Table 1).

If geometry optimizations of *RS*-CAT are performed without dispersion corrections, three extended conformers are favored, where the indole ring in the tryptophan side chain is far away from the DKP ring (Supporting Information, Figure S1). In the spectral analysis, however, these conformations provide poor agreement with experiment (vide infra).

Also for *SS*/*RR*-CAT geometries, B3LYP-D predicts that folded conformers are preferred over extended ones. The six most stable *SS* conformers (Figure 3), their relative energies, Boltzmann weights, and selected hydrogen-bonded parameters are listed in Table 2. In *SS*/*RR*-CAT, the arginine and tryptophan side chains are located on the same side of the DKP ring, giving rise to even more extended $C_{\beta/\delta}H\cdots\pi$, NH···$\pi$ and NH···O interactions than for *RS*-CAT (Figure 2). As for the *RS* isomer, ZPVE contributions lead to changes in the conformer ordering. The lowest-energy conformer (b1) of *SS*-CAT has a Boltzmann weight of 65%; its folded structure is stabilized by a $C_\delta H\cdots\pi$ interaction and an NH···O hydrogen bond. The second-most stable conformer (b2) is stabilized by intramolecular $C_\beta H\cdots\pi$ and NH···O interactions, and has a relative energy of 0.84 kcal/mol with a population of 16%. The other four conformers account for 19% of the population only. As for the similar CATM compound,[29] nonbonding interactions between the side chains thus play a major role in the structural stabilization of CAT.

The DKP ring conformation is important for supramolecular architecture and molecular recognitions.[17,81] We analyzed its geometry by means of the ring-puckering coordinates (Q, θ, and P_2) based on the Haasnoot's truncated Fourier formalism.[82] A six-membered ring can exist in a variety of conformations, e.g., planar (P), boat (B), twist-boat (T), chair (C), half-chair (H), envelope (E), and screw-boat (S). All of these conformations can be represented by the endocyclic torsion angles ϕ_j (j = 0 − 5, Figure 1a). The calculated ring-puckering coordinates for *RS*- and *SS*-CAT are listed in Tables 1 and 2, respectively. As can be seen from Table 1, the DKP

dx.doi.org/10.1021/jp311151h | J. Phys. Chem. A 2013, 117, 1721−1736

Table 1. Relative Energies (ΔE, kcal/mol), Boltzmann Weights (BW, 298 K), the $C_{\alpha/\delta}H\cdots\pi$ Distances[a] ($d_{CH\cdots\pi}$, Å), the NH···O Distances (r_1, Å), and Pseudorotational Parameters (Q, θ, and P_2, deg) of Stable *RS*-CAT Conformers (B3LYP-D/6-31++G/IEFPCM(methanol))**

						pseudorotational parameters			
conformer	ΔE	ΔE_0[b]	BW[c]	$d_{C-H\cdots\pi}$	r_1	Q	θ	P_2	shape[e]
a1	0.00	0.00	0.61	2.572	1.789	33	88	229	T
a2	0.49	0.66	0.20	2.558	1.785	33	93	224	T
a3	0.83	1.07	0.10	2.528	1.769	35	92	228	T
a4	0.95	1.52	0.05	2.499	1.753	36	97	225	T
a5	0.55	1.64	0.04	2.446/2.614[d]		36	91	224	T

[a] $d_{CH\cdots\pi}$ is the distance between H and the center of the five- (or six)-membered ring of the indole group. [b] ΔE_0 includes zero-point vibrational energy (ZPVE). [c] BWs were calculated on the basis of the ΔE_0. [d] The 2.614 Å is the C_δ–H···π distance of the a5 conformer. [e] T = twist-boat.

Table 2. Calculated Energies and Geometry Parameters (Definitions in Table 1 and Figure 3) of Stable *SS*-CAT Conformers

								pseudorotational parameters			
conformer	ΔE	ΔE_0	BW	$d_{C-H\cdots\pi}$	$d_{N-H\cdots\pi}$	r_1	r_2	Q	θ	P_2	shape
b1	0.00	0.00	0.65	2.399		1.834		11	33	152	C → P
b2	1.27	0.84	0.16	2.351		1.747		22	96	232	T
b3	0.75	1.13	0.10		2.350	1.883	2.573	6	82	193	T → P
b4	1.42	1.73	0.03	2.560/2.525		1.775		23	91	232	T
b5	1.19	1.83	0.03	2.399		1.782		22	86	233	T
b6	0.77	1.87	0.03	2.397		2.284	1.865	10	14	159	C → P

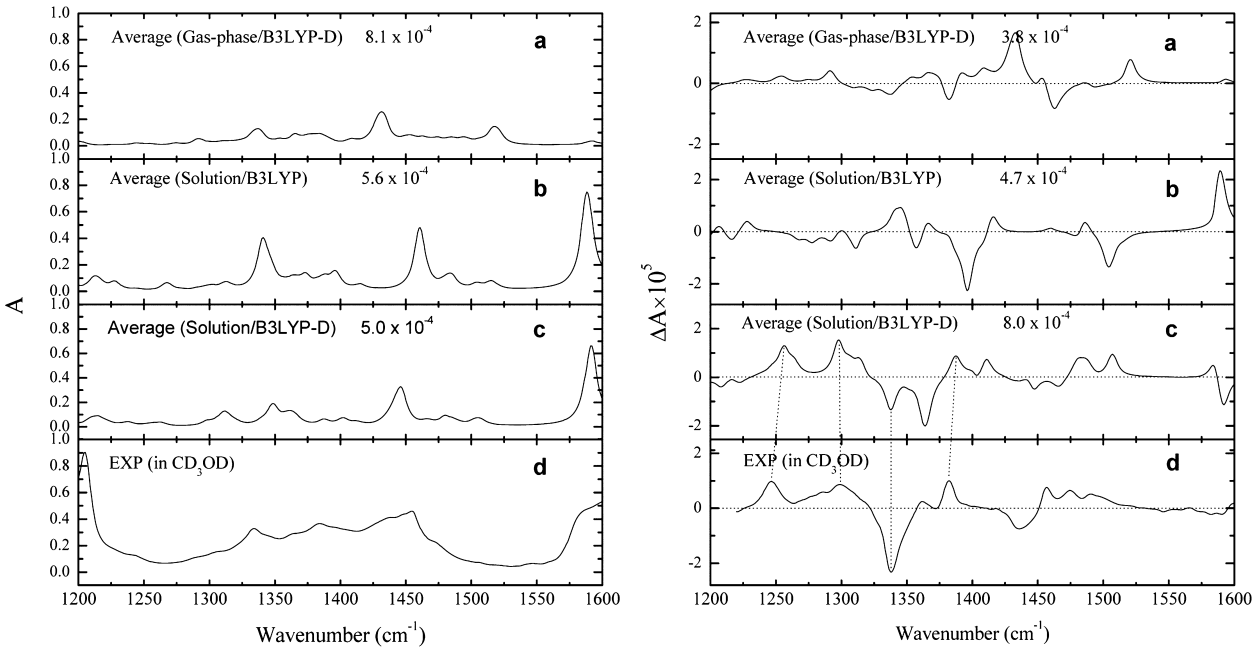

Figure 4. IR (left) and VCD (right) calculated and experimental spectra of *RS*-CAT (CD_3OD solution): (a) B3LYP-D/6-31++G** (gas phase); (b) B3LYP/6-31++G**/IEFPCM(methanol); (c) B3LYP-D/6-31++G**/IEFPCM(methanol); (d) experiment.

ring of *RS*-CAT has θ close to 90° with deviations up to 7°; the P_2 values are in the range 224–229°. The conformation of the DKP ring in *RS*- and *SR*-CAT is assigned to a twist-boat (T) conformation, "down" for *RS* and "up" for *SR*. This conformation is almost independent of the orientations of the indole group and arginine side chains.

For *SS*-CAT, the conformational variations are larger than for *RS*-CAT (Table 2). For example, the b2–b5 structures adopt a twist-boat-down conformation; however, the b3 structure is almost planar (P), the puckering amplitude being about 6°. The b1 and b6 structures have the same chair (C) conformation and very small amplitudes, less than 12°. This again shows a weak correlation between the DKP ring conformation and orientation of the side chains.

IR Absorption and VCD Spectra. To determine a reliable computational protocol, we tested the dependence of the averaged IR and VCD spectra on the inclusion of the solvent and dispersion corrections through comparison with measured experimental data for *RS*-CAT (Figure 4). Three levels of theory (B3LYP-D/6-31++G**(gas phase), B3LYP/6-31++G**/IEFPCM(methanol), and B3LYP-D/6-31++G**/IEFPCM(methanol), with relative energies and Boltzmann weights listed in Table S1 of Supporting Information) were employed for optimizations and subsequent IR/VCD calcu-

dx.doi.org/10.1021/jp311151h | J. Phys. Chem. A 2013, 117, 1721–1736

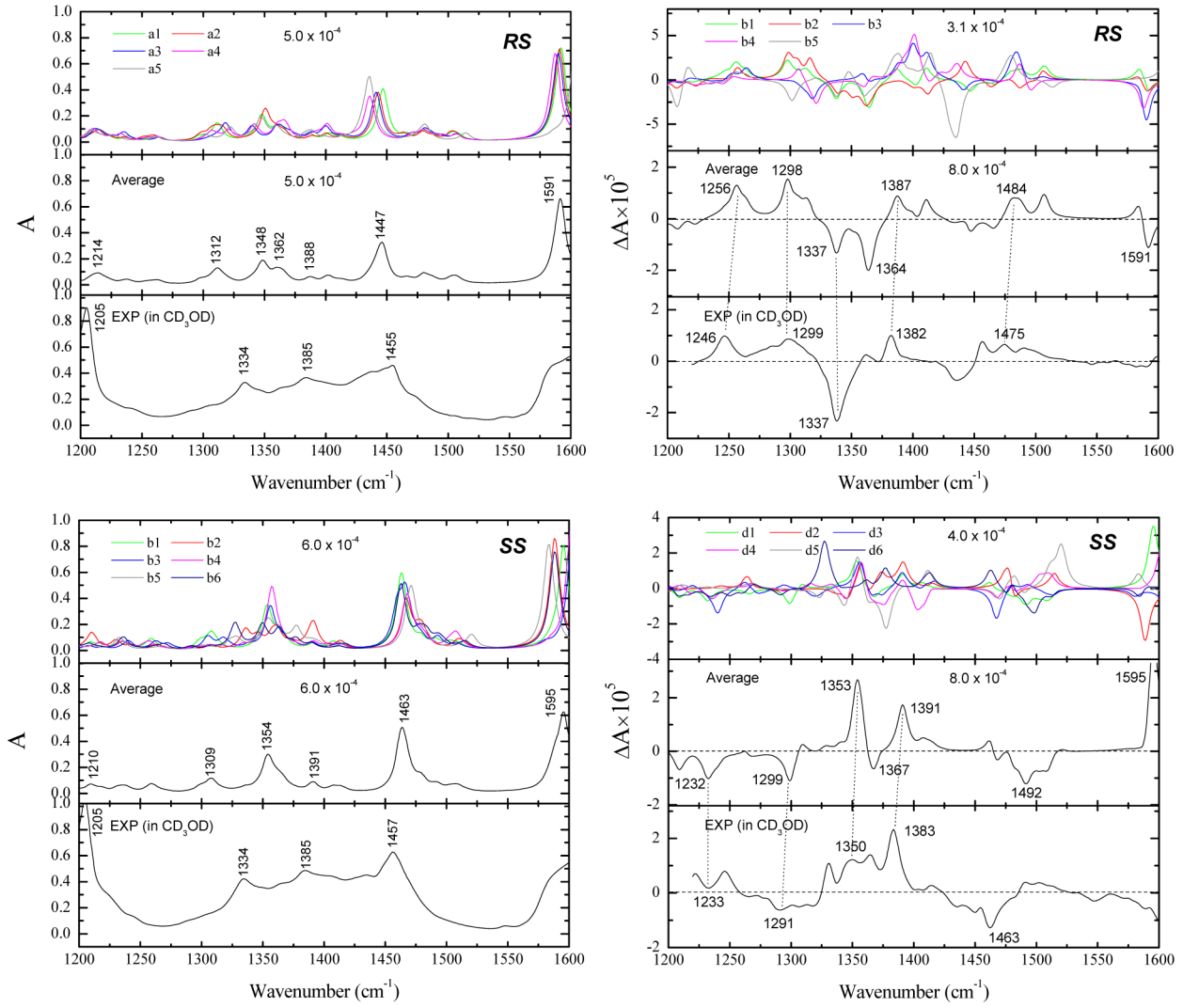

Figure 5. Calculated (B3LYP-D/6-31++G**/IEFPCM(methanol), top and middle panels, corrected for deuterium exchange) and experimental (in CD_3OD, bottom) IR (left) and VCD (right) spectra of *RS*- and *SS*-CAT stereoisomers.

lations (Figure 4). The importance of solvent corrections is apparent by comparison of the calculations in the gas phase, and with the implicit IEFPCM solvent model (Figure 4, panels a and c). Similarly, DFT-D leads to better results than plain DFT (Figure 4, panels b vs c). In particular, the VCD results show that inclusion of dispersion significantly improves agreement with experiment. The hybrid DFT-D functional with the IEFPCM solvent model thus appears to be an effective method for VCD calculations of CAT, in agreement with previous studies.[29,83]

The calculated DFT-D IR and VCD spectra of *RS*- and *SS*-CAT are compared to experiment in Figure 5. Vibrational wavenumbers and assignments of the main theoretical and experimental peaks are compiled in Table 3. The averaged theoretical IR spectra are in a good agreement with the main peaks of the corresponding experiment for both CAT isomers. The IR subspectra of the different conformers show minor differences, mainly in the peak intensities. Note that the experimental IR peak around 1205 cm^{-1} is assumed to originate from the trifluoroacetic acid (TFA) counterion of CAT.

The experimental VCD spectra show reliable results in the region 1500−1240 cm^{-1}. Due to the limited amount of sample, it was not possible to obtain the carbonyl stretching region (around 1670 cm^{-1}), which, however, is expected to provide less information about molecular structure than the lower-frequency region. The computed subspectra of the different conformers show that the simulated VCD features are more dependent on the conformational state than IR. The main peaks in the averaged theoretical VCD spectra are (+) 1256, (+) 1298, (−) 1337, (−) 1364, (+) 1387, and (+) 1484 cm^{-1} for *RS*-CAT (Figure 5, top right, panel 2), and (−) 1232, (−) 1299, (+) 1353, (−) 1367, (+) 1391, and (−) 1492 for *SS*-CAT (Figure 5, bottom right, panel 2).

The calculated positive VCD peak at 1298 cm^{-1} for *RS*-CAT corresponds mainly to C−H bending vibrations of the arginine and matches the experimental band at 1299 cm^{-1}. Likewise, for *SS*-CAT, the computed negative peak at 1299 cm^{-1} matches the experimental peak at 1291 cm^{-1}. This band can be employed to assign the configuration at C_1 of CAT (+ for *R*, − for S); however, the experimental peak in the *SS*-CAT spectrum is not very strong. The calculated 1337 cm^{-1} VCD band for *RS*-CAT (1334 cm^{-1} in the IR spectrum) corresponds to the observed peak at 1337 cm^{-1} and is also dominated by C−H bending vibrations. Similarly, for *SS*-CAT, the strong positive VCD band at 1353 cm^{-1} corresponds to the experimental 1350 cm^{-1} peak. The calculated positive peaks

dx.doi.org/10.1021/jp311151h | J. Phys. Chem. A 2013, 117, 1721−1736

Table 3. Selected Vibrational Bands and Experimental and Calculated Positions (cm^{-1})

exp		B3LYP/6-31++G**/IEEPCM		
RS/SR	*SS/RR*	*RS/SR*	*SS/RR*	assignment[a]
		Raman		
1547	1549	1582	1582	ν C=C (Trp)
1436	1436	1455	1456	ν C=C, ν C—N (Trp), δ CH, δ NH (Trp)
1363	1363	1386	1389	δ CH
1241	1244	1245	1246	δ CH, δ NH (DKP ring and Trp)
1195	1203	1195	1206	δ CH, Arg deformation
1011	1013	1022	1023	ν C—C (Trp)
925	931	937	940	CH_2 wagging
877	876	882	880	ν C=C (Trp, ring deformation)
837	838	837	838	CH (Trp) out-of-plane deviation
758	758	764	767	ν C=C (Trp, breathing mode)
672	679	672	681	NH (DKP ring) out-of-plane deviation, DKP ring deformation
541	543	562	570	NH (DKP ring) out-of-plane deviation, Trp ring deformation
202	202	210	202	NH_2 Arg out-of-plane wagging
160	162	166	155	NH_2 Arg and NH (DKP ring) out-of-plane wagging
		IR[b]		
1604	~1595[c]	1591	1595	ν C=C (Trp)
1455	1457	1447	1463	ν C—N (DKP, "amide III")
1385	1385	1388	1391	δ CH
1334	1334	1348	1354	δ CH, ν C—N (DKP)
1299[d]	1291[d]	1298	1299	δ CH, ν C—N (DKP)

[a]Typical modes; abbreviations: ν, stretching; δ, bending. [b]Experimental and computed averaged peaks. [c]Shoulder. [d]VCD band.

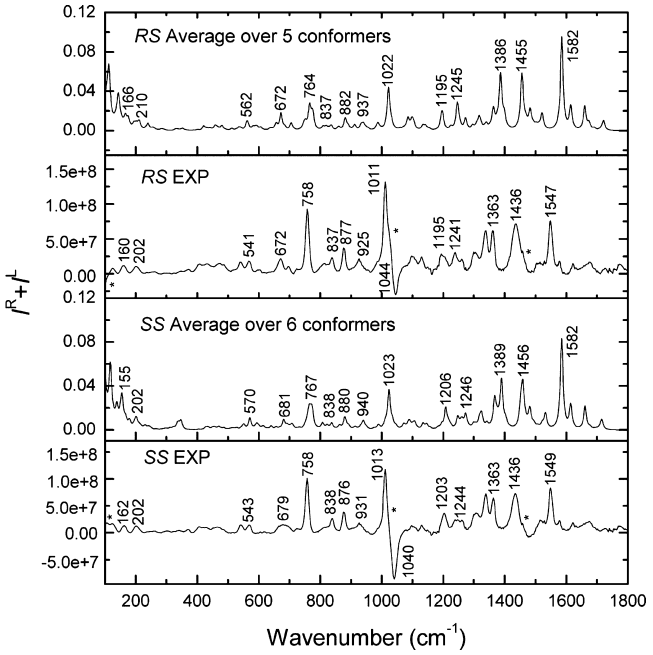

Figure 6. Calculated (B3LYP-D/6-31++G**/IEFPCM/methanol, panel 1 and 3 from the top) and experimental (panel 2 and 4) Raman spectra of *RS* and *SS* CAT stereoisomers. In experiment, bands close to an asterisk (*) may be affected by the methanol solvent. The negative signal at 1040–1044 cm^{-1} is an artifact due to the baseline subtraction.

at 1387 (for *RS*-CAT) and 1391 (for *SS*-CAT) cm^{-1} come mainly from the contribution of C–H bending in the tryptophan part. This band is characteristic for the chiral center at C_4 (+ for *S*, − for *R*).

Overall, the theoretical modeling explains the relation between AC and the spectral response reasonably well, although accurate reproduction of all VCD features clearly still remains challenging. Nevertheless, the two VCD bands at 1298/1299 and 1387/1391 cm^{-1} can serve as characteristic peaks for the C_1 and C_4 chiral centers of CAT, allowing for a full AC determination.

Raman and ROA Spectra. The calculated and experimental DFT-D Raman spectra of *RS*- and *SS*-CAT stereoisomers in methanol show similar Raman intensity profiles (Figure 6, Table 3). However, attempts to measure the Raman optical activity (ROA) of CAT led to very noisy spectra (Figure S2, Supporting Information), not only due to the instability of tryptophan-containing samples in the laser beam but also due to the low ROA/Raman circular intensity difference (CID) ratios of most vibrational transitions (except those below 200 cm^{-1}). A comparison of the experimental ROA to computation thus provides very limited information. For example, the computation reproduces the main experimental ROA features around 100–200 cm^{-1} (Figure S2, Supporting Information). These are, however, similar in *RS* and *SS* compounds.

On the other hand, calculated Raman intensities can be related to experiment within the entire range of frequencies. The C=C stretching vibrations in the tryptophan side-chain dominate the strong bands computed at 1582 cm^{-1} for both isomers (experimentally 1547 and 1549 cm^{-1} for *RS*-CAT and *SS*-CAT, respectively). The Raman band simulated at 1386 cm^{-1} (experimentally 1363 cm^{-1}) corresponds mainly to C–H bending. These bands are also visible in the theoretical IR spectra (Figure 5).

The vibrational spectra around 1200 cm^{-1} are very similar to those of the cyclo(Arg-Tyr(OMe)) (CATM) analogue of CAT,[29] whereas the bands simulated at 1022/1023 and 764/767 cm^{-1} are specific for the indole group in CAT.[84] The weak Raman bands calculated at 672/681 and 562/570 cm^{-1} involve NH out-of-plane deviations in the DKP ring. The Raman bands in the low-wavenumber region (around 160 and 200 cm^{-1}), traditionally considered difficult to simulate and measure, are also reproduced in the simulations. They mainly originate from NH_2 out-of-plane wagging.

The Raman spectra can even provide tentative information about the configuration of CAT. Some small frequency shifts measured for the *RS* and *SS* isomers seem to be reproduced in the theoretical spectra. For example, the experimental bands at 672, 925, and 1195 cm^{-1} in the Raman spectrum of *RS*-CAT move to 679, 931, and 1203 cm^{-1} for *SS*-CAT (Figure 6). This shift is reproduced by the calculation as 672, 937, and 1195 (*RS*-CAT) → 681, 940, and 1206 cm^{-1} (*SS*-CAT). This information could tentatively be used to distinguish between diastereomers of CAT.

ECD Spectra. To test the applicability of ECD for AC determination, and to assess the reliability of theoretical ECD spectra, we performed TD-DFT computations with three different functionals (B971, B3LYP, and CAM-B3LYP, all in combination with the IEFPCM solvent model) employing the dispersion-corrected CAT geometries and compared the results to experiment (Figure 7).

The B971 and B3LYP functionals slightly overestimate the wavelength of the main negative band (at 215 nm in

dx.doi.org/10.1021/jp311151h | J. Phys. Chem. A 2013, 117, 1721–1736

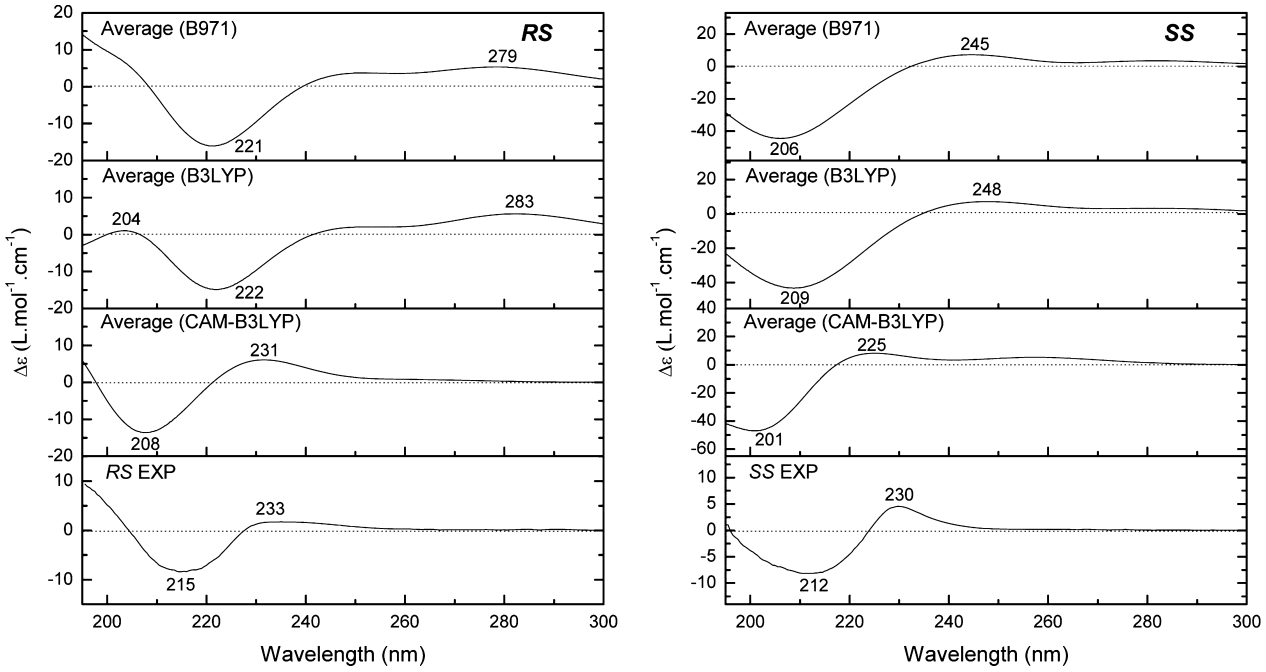

Figure 7. Comparison of the calculated (TD-B971/6-31++G**/IEFPCM(methanol), TD-B3LYP/6-31++G**/IEFPCM(methanol), and TD-CAM-B3LYP/6-31++G**/IEFPCM(methanol), panes 1−3, respectively) and experimental ECD spectra (in methanol, panel 4) for *RS*- (left) and *SS*-CAT (right) stereoisomers.

experiment) of *RS*-CAT, by 6 and 7 nm, respectively, whereas CAM-B3LYP underestimates it by 7 nm (Figure 7). CAM-B3LYP also reproduces the weak experimental peak at 233 nm (theoretically 231 nm). For wavelengths larger than ∼250 nm, the B971 and B3LYP functionals give false maxima at 279 and 283 nm. Similarly, for *SS*-CAT, the CAM-B3LYP functional generates the smallest mean deviation of 8 nm when compared to the main experimental peaks. Overall, CAM-B3LYP gives the best results in this case. A good performance of this functional was also observed in previous studies.[85−88] Note that the Coulomb-attenuating method (CAM)[89] used therein ensures that charge-transfer states are properly treated, which appears important for CAT. The strong negative CAM-B3LYP ECD peak at 208 nm originates from a HOMO−1 → LUMO+2 transition (traditionally described as $\pi \rightarrow \pi^*$ amide transition) involving contributions from the indole and DKP rings, whereas the relatively weak positive peak at 231 nm originates mainly from a HOMO → LUMO+2 ($\pi \rightarrow \sigma^*$ amide) transition, involving the indole ring, protonated guanidine group, and from a small contribution of HOMO → LUMO ($\pi \rightarrow \pi^*$) on the indole ring.

The HOMO and LUMO orbitals of the a1 conformer of *RS*-CAT plotted in Figure 8 also illustrate the different behavior of the B3LYP and CAM-B3LYP functionals. B3LYP predicts that both the HOMO and LUMO are located on the indole ring of the tryptophan side chain, whereas the CAM-B3LYP HOMO is located on the indole ring and the LUMO is on the protonated guanidine group. This may explain the false signal around 283 nm obtained by B3LYP.

The influence of the geometry on the ECD spectrum is investigated in Figure 9a (panel 1) by comparing calculations on the dispersion-corrected (B3LYP-D) and the dispersion-free (B3LYP) *RS*-CAT geometries. Whereas the B3LYP-D geometries provide good agreement with experiment, ECD calculations on the uncorrected B3LYP geometries provide a different spectral shape, with a wide positive band at 253 nm

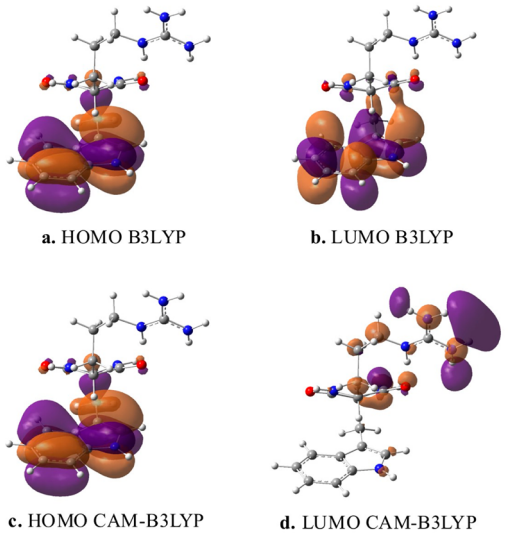

Figure 8. Calculated HOMO and LUMO orbitals of the a1 conformer of the *RS*-CAT stereoisomer using B3LYP and CAM-B3LYP functionals (isodensity surface 0.02 e/au^3).

(originating from a HOMO → LUMO+1 ($\pi \rightarrow \pi^*$) transition, occurring predominantly on the indole ring). A similar behavior was observed for *SS*-CAT, where we show the CAM-B3LYP//B3LYP-D results only (Figure 9a, panel 3). The calculated negative peak at 201 nm (originating from a HOMO−1 → LUMO+1 ($\pi \rightarrow \pi^*$) transition associated with the indole ring) can be assigned to the experimental peak at 212 nm. The weak positive experimental peak at 230 nm is also well reproduced by the CAM-B3LYP calculation. The strong negative experimental peaks at 215 nm for *RS*-CAT and 212 nm for *SS*-CAT can be used to assign the chiral center at C_4 as *S*. The chiral center at C_1 is silent and a full assignment of the absolute configuration of CAT on basis of ECD is therefore not possible.

dx.doi.org/10.1021/jp311151h | J. Phys. Chem. A 2013, 117, 1721−1736

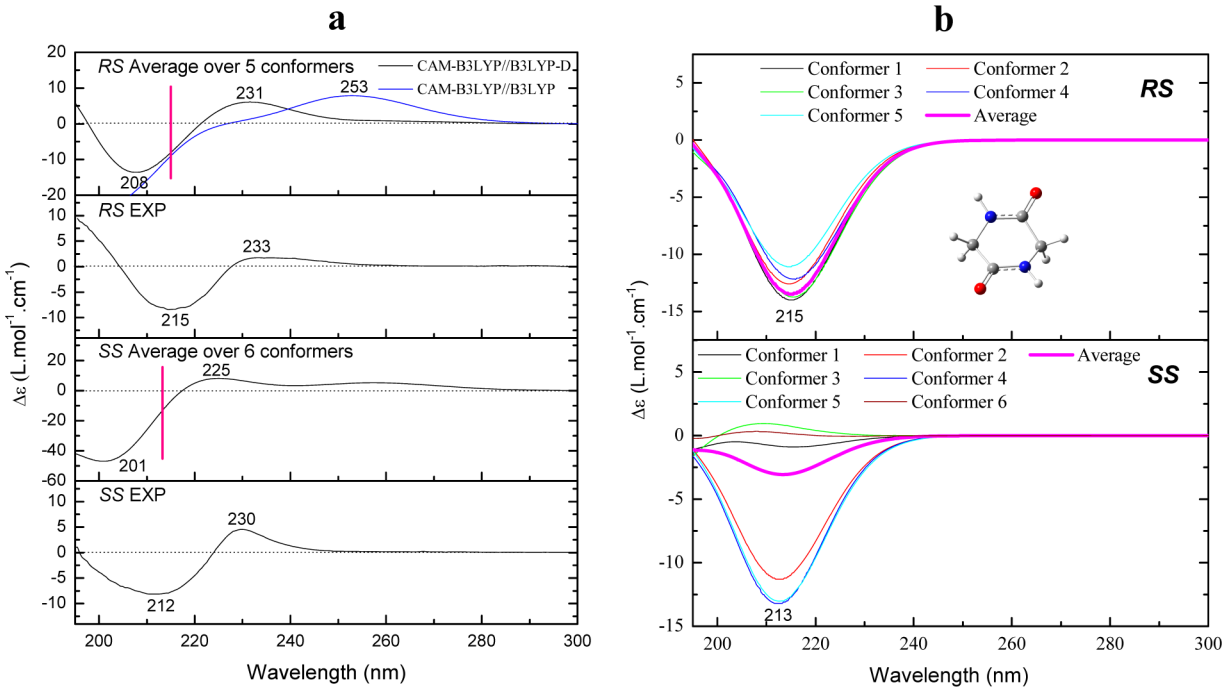

Figure 9. (a) Calculated (TD-CAM-B3LYP//B3LYP-D/6-31++G**/IEFPCM(methanol), panels 1 and 3) and experimental (in methanol, panels 2 and 4) ECD spectra for the *RS*- and *SS*-CAT stereoisomers. In panel 1 (left), the TD-CAM-B3LYP//B3LYP *RS* ECD spectrum (blue line) is also shown. Pink lines indicate the "amide" bands. (b) ECD spectra of cyclo(Gly-Gly) calculated at the same theoretical level.

Table 4. ^{1}H NMR Assignments for CAT[a]

	SS-CAT			*RS*-CAT		
no.[b]	experiment δ_H (mult, J in Hz)	theory δ_H	E[c] δ_H	experiment δ_H (mult, J in Hz)	theory δ_H	E[c] δ_H
1	3.68 (ddd, J = 7.7, 5.2, 1.5)	3.98	0.30	2.77 (m)	1.17	−1.60
2	8.01[d] (d, J = 2.3)	5.04	−2.97	7.92[d] (s)	4.45	−3.47
4	4.31 (ddd, J = 4.8, 3.7, 1.3)	4.42	0.11	4.23 (ddd, J = 4.8, 4.0, 1.1)	4.11	−0.12
5	8.10[d] (d, J = 2.4)	5.95	−2.15	8.11[d] (d, J = 2.3)	5.89	−2.22
7′	0.49[e] (m)	1.18	0.69	1.44 (m)	1.25	−0.19
7″	0.87[e] (m)	0.82	−0.05	1.67 (m)	1.23	−0.44
8′/8″	0.79 (m)	−0.03	−0.82	1.44 (m)	1.32	−0.12
9′/9″	2.62 (td, J = 7.0, 2.0)	2.46	−0.16	3.04 (t, J = 6.9)	2.81	−0.23
10	7.21[d] (t, J = 5.7)	6.14	−1.07	7.44[d] (t, J = 5.8)	8.28	0.84
12′	3.14[e] (dd, J = 14.7, 4.6)	3.17	0.03	3.15 (ddd, J = 14.7, 4.5, 0.7)	3.08	−0.07
12″	3.49[e] (dd, J = 14.8, 3.6)	4.46	0.97	3.47 (ddd, J = 14.7, 3.9, 0.7)	3.70	0.23
14	7.08 (s)	7.28	0.20	7.06 (s)	7.16	0.09
15	10.86[d] (d, J = 2.3)	8.11	−2.75	10.91[d] (m)	8.17	−2.74
18	7.63 (dd, J = 8.0, 1.0)	7.88	0.25	7.60 dt, J = 8.0, 1.0)	8.02	0.42
19	7.01 (ddd, J = 8.0, 7.0, 1.0)	7.43	0.42	7.00 (ddd, J = 8.0, 7.0, 1.0)	7.38	0.38
20	7.09 (ddd, J = 8.0, 7.0, 1.1)	7.37	0.28	7.08 (ddd, J = 8.2, 7.0, 1.2)	7.46	0.38
21	7.34 (d, J = 8.1)	7.63	0.29	7.33 (dt, J = 8.1, 0.9)	7.65	0.32
AAE[f]			*0.35*			*0.35*

[a]Measured at 600 MHz in methanol-d_4 (DMSO-d_6 for acidic protons), [b]See Figure 1 for atom labeling, [c]E = Error. [d]Correlations only seen in DMSO-d_6. [e]The individual hydrogen assignments for 7′/7″ and 12′/12″ were based on the ROESY crosspeak volumes to the nearest N−H proton on the DKP ring in DMSO-d_6. [f]Average absolute error, not including acidic protons on N_2, N_5, N_{10}, and N_{15}.

To better understand the link between the ECD signal and the dipeptide structure, we substituted the side chains of CAT with hydrogen atoms, forming cyclo(Gly-Gly) (cGG). The calculated ECD spectra of cGG are shown in Figure 9b. Clearly, the amide electronic system primarily contributes to the bands at 215 and 213 nm for the *RS* and *SS* stereoisomers, respectively. For CAT, the positions of the "amide" bands at 215 and 213 nm are labeled with a pink line in Figure 9a. The strong negative bands of the amide ECD in cGG originate from the twist-boat (T) DKP ring conformation; close-to-planar forms give rather weak ECD signals. By comparing the CAT and cGG spectra, we can speculate that in *RS*-CAT, the amide signal appears weakened by a coupling to the side chain, whereas it is strengthened in *SS*-CAT.

To document the role of the peptide side chains on the ECD signal, we compared the CAT spectra to that of CATM; a previously studied analogue (Figure S3, Supporting Information).[29] In CATM, the tryptophan is replaced by a methylated

dx.doi.org/10.1021/jp311151h | J. Phys. Chem. A 2013, 117, 1721−1736

(−OMe) tyrosine. Both the *RS*-CATM and *RS*-CAT stereoisomers have a negative ECD peak at 208/218 nm (Figure S3, Supporting Information), but otherwise the spectra are quite different, reflecting the sensitivity of ECD to structural changes. The *SS*-CAT and *SS*-CATM spectra also exhibit very different features. Thus although the glycine model (Figure 9b) suggest a limited locality of CD, the side-chain influence in CAT/CATM highlights the known difficulty in deriving reliable empirical rules for AC determination based on ECD studies of structurally related compounds.

NMR Analysis. Experimental and theoretical NMR ^{1}H and ^{13}C chemical shifts, J(C,H) coupling constants and ^{1}H,^{1}H NOE correlations were also analyzed with respect to the stereochemical assignment of CAT. The measurements were performed in CD_3OD and in DMSO-d_6; the computations were done with dispersion-corrected geometries for *SS*- and *RS*-CAT, and conformers were averaged on the basis of the Boltzmann populations.

The ^{1}H chemical shifts are sensitive to conformational changes and neighboring nuclei as well as solvent effects. This makes each proton chemical shift a sensitive probe for its environment, but at the same time accurate calculations become challenging. The experimental ^{1}H chemical shifts for *RS* and *SS*-CAT in CD_3OD are given in Table 4 (acidic protons were determined in DMSO-d_6, as they are invisible in CD_3OD due to exchange with deuterium). Qualitative inspection of the proton chemical shifts reveals a strong upfield shift of the arginine side chain resonances in the *SS/RR* pair compared to the *RS/SR* pair. This is characteristic for protons being shielded by a stacking interaction with an aromatic ring moiety, such as the indole ring of CAT. The experimental ^{1}H shifts show generally good agreement with computed values, except for acidic protons (Table 4). The individual hydrogen assignments for the pairs 7′/7″ and 12′/12″ were based on the ROESY cross peak volumes to the nearest N−H proton on the DKP ring in DMSO-d_6. For both proton pairs, the individual distances C−H_X···H−N (where X = 7′ and 7″ or 12′ and 12″) predicted by the dominant *RS*- and *SS*-CAT DFT structures differed by more than 1.1 Å from each other and the cross peak volumes all were sufficiently different to allow explicit assignment of the geminal protons. The average absolute error (AAE) of the theoretical ^{1}H values obtained in methanol (not including acidic protons obtained in DMSO) is low, 0.35 ppm for both *SS*- and *RS*-CAT (Table 4).

The recorded ^{1}H chemical shifts that show the largest differences between the diastereomers are observed for H_1, $H_{7'}$, $H_{7''}$, $H_{8'/8''}$, and $H_{9'/9''}$. The experimental and theoretical $\Delta\delta_{RS\text{-}SS}$ values for these are (experiment; theory) H_1(−0.91; −2.81), $H_{7'}$ (0.95; 0.07), $H_{7''}$ (0.80; 0.41), $H_{8'/8''}$ (1.35; 0.66), $H_{9'/9''}$ (0.42; 0.35). Thus, although the sign of $\Delta\delta_{RS\text{-}SS}$ is reproduced correctly for all of these shieldings, the computed values are considerably overestimated for H_1, and somewhat underestimated for $H_{7'}$ and $H_{8'/8''}$.

The theoretical ^{13}C shifts also reasonably well agree with experiment, with AAEs of 5.30 for *SS*-CAT and 7.05 for *RS*-CAT (Table 5). The largest errors are observed for the C(=O) carbons (C_3 and C_6), possibly due to the lack of explicit hydrogen bonding from solvent molecules to the carboxyl group and/or the neighboring NH group in the calculations. In the experimental ^{13}C spectra, C_1, C_7, C_{13}, C_{17}, and C_{18} exhibited the most substantial differences between the diastereomers. The $\Delta\delta_{RS\text{-}SS}$ values for these are (experiment; theory) C_1 (2.34; 1.60), C_7 (3.94; 3.50), C_{13} (2.11; 0.48), C_{17} (2.05; 0.71), and C_{18} (1.96; −0.56). The sign is thus reproduced for most cases, together with the magnitude for the major difference at C_7. However, the theory also predicts a large $\Delta\delta_{RS\text{-}SS}$ for C_3 (6.05), not supported by experiment (0.05). Overall, the $\Delta\delta_{RS\text{-}SS}$ values are small compared to the absolute values of the carbon shifts, which is not surprising as ^{13}C nuclei are relatively electron rich and their chemical shifts are therefore dominated by the chemical bonds formed with neighboring nuclei.

Table 5. ^{13}C NMR Assignments for CAT[a]

	SS-CAT			*RS*-CAT		
no.[b]	experiment δ_C	theory δ_C	E[c] $\Delta\delta_C$	experiment δ_C	theory δ_C	E[c] $\Delta\delta_C$
1	55.17	61.65	6.48	52.83	60.05	7.22
3	169.87	175.11	5.24	169.93	181.15	11.22
4	57.49	64.40	6.91	56.24	64.55	8.31
6	169.48	177.79	8.31	168.86	179.14	10.28
7	32.06	33.91	1.85	28.12	30.41	2.29
8	24.53	25.16	0.63	22.86	26.28	3.42
9	41.72	45.42	3.70	40.52	44.93	4.41
11	158.44	159.74	1.30	157.10	160.00	2.90
12	30.48	34.92	4.44	29.69	35.62	5.93
13	109.66	117.07	7.41	107.55	116.59	9.04
14	126.07	132.34	6.27	124.66	133.16	8.50
16	137.80	143.17	5.37	136.48	143.74	7.26
17	129.38	135.88	6.50	127.33	135.16	7.83
18	120.28	126.08	5.80	118.32	126.64	8.32
19	120.22	127.33	7.11	118.75	126.55	7.80
20	122.54	129.55	7.01	121.14	129.31	8.17
21	112.18	118.03	5.85	110.74	117.72	6.98
AAE[d]			5.30			7.05

[a]Measured at 151 MHz in CD_3OD, [b]See Figure 1 for atom labeling, [c]E = error. [d]Average absolute error.

For selected C,H pairs in CAT, in particular those involving the chiral centers, experimental and theoretical long-range J(C,H) coupling constants were obtained in CD_3OD, as shown in Table 6 (see also Supporting Information Figure S4). The sign of the experimental constants is not known. The theoretical J's are positive for ^{3}J(C,H) and negative for ^{2}J(C,H) values. AAEs for the six evaluated coupling constants are 1.07 Hz for *SS*-CAT and 0.94 Hz for *RS*-CAT. The error of the experimental CH couplings is estimated to be 0.4−0.5 Hz. Only differences between the theory and experiment exceeding one Hertz therefore indicate limitations in the computational method.

Four of the six experimental J's show differences of more than 1 Hz between the two diastereomers; the absolute experimental and theoretical $\Delta J_{RS\text{-}SS}$ values for these are [experiment; theory] $^{3}J(C_3,H_1)$ [2.15;1.54], $^{3}J(C_3,H_{12''})$ [1.58;0.05], $^{2}J(C_6,H_1)$ [1.44;1.86], and $^{3}J(C_6,H_4)$ [1.87;3.71]. The magnitudes of the differences are thus reproduced reasonably well, except for $^{3}J(C_3,H_{12''})$. *SS*-CAT has larger experimental J's than *RS*-CAT for $^{3}J(C_3,H_1)$, $^{3}J(C_3,H_{12'})$, $^{3}J(C_3,H_{12''})$, and $^{2}J(C_6,H_1)$, whereas the J's for *RS*-CAT are larger for J's involving H_4, $^{2}J(C_3,H_4)$ and $^{3}J(C_6,H_4)$. In all cases, theory correctly predicts the diastereomer with the larger J. Thus, if two unknown CAT isomers are compared, the relative J(C,H) coupling constants provide assignment of the enantiomeric pair (*SS/RR* or *RS/SR*). In combination with, e.g., ECD, providing the absolute configuration for the C_4 center, this would yield full AC assignment.

dx.doi.org/10.1021/jp311151h | J. Phys. Chem. A 2013, 117, 1721−1736

Table 6. J(C,H) Coupling Constants (Hz) in CD_3OD for CAT

	SS-CAT			*RS*-CAT		
J(C,H)[a]	experiment[b]	theory	AE[c]	experiment	theory	error
$^3J(C_3,H_1)$	|3.41|	1.82	1.59	|1.25|	0.28	0.97
$^2J(C_3,H_4)$	|7.49|	−5.93	1.56	|7.53|	−6.67	0.86
$^3J(C_3,H_{12'})$	|7.41|	7.36	0.05	|7.18|	7.35	0.17
$^3J(C_3,H_{12''})$	|2.38|	1.31	1.07	|0.8|	1.26	0.46
$^2J(C_6,H_1)$	|7.85|	−6.3	1.55	|6.41|	−4.44	1.97
$^3J(C_6,H_4)$	|3.71|	3.09	0.62	|5.58|	6.80	1.22
AAE[d]			1.07			0.94

[a]See Figure 1 for atom labeling. [b]Sign could not be determined. [c]Absolute error. [d]Average absolute error.

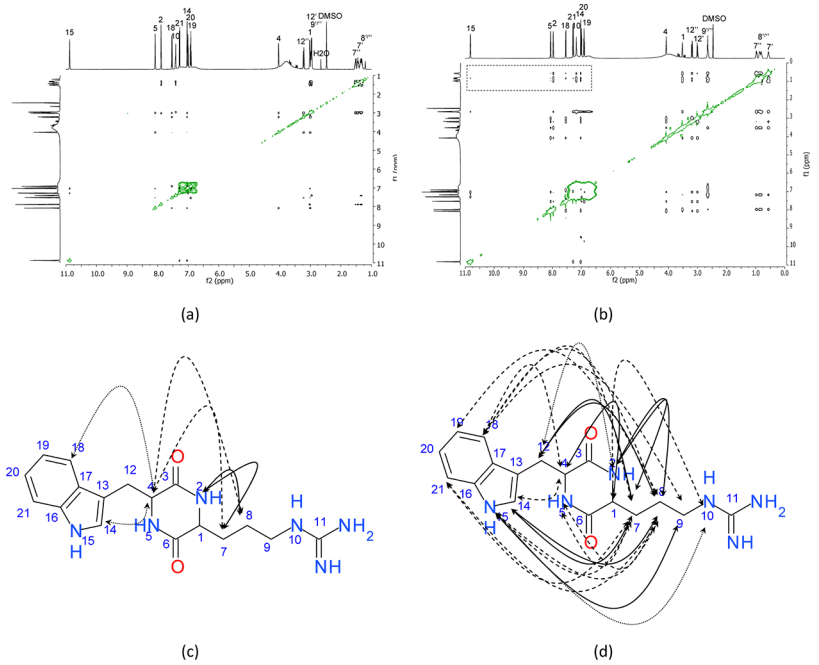

Figure 10. ROESY (300 ms spinlock duration) spectra of (a) the *RS/SR* and (b) the *SS/RR* enantiomer pairs in DMSO-d_6. Key long-range through space correlations are displayed below the respective spectra (c and d), qualitatively classified as strong (solid lines), medium (dashed lines), or weak (dotted lines). Most significantly, a set of additional cross peaks between the aromatic tryptophan and the aliphatic arginine resonances are present in the *SS/RR* enantiomer pair but not the *RS/SR* pair (dashed box).

Assignment of the relative configuration of a single unknown CAT isomer on basis of the J(C,H) coupling constants appears more challenging. The experimental J's for *SS*-CAT yield an AAE of 1.94 Hz with the theoretical J's for *RS*-CAT, compared to an AAE of 1.07 Hz obtained with the *SS*-CAT theoretical J's (Table 6). This would correctly identify *SS*-CAT as belonging to the *SS/RR* enantiomeric pair. However, the experimental J's for *RS*-CAT yield an AAE of 0.91 Hz with the theoretical J's for *SS*-CAT, which is essentially the same as with the *RS*-CAT theoretical results (AAE = 0.94 Hz). Therefore, assignment of *RS*-CAT to a given enantiomeric pair on the basis of the J coupling constants alone would not be possible.

The ROESY spectra used for assignment of the CAT isomers in DMSO-d_6 are shown in Figure 10. The corresponding NOESY spectra with mixing times between 200 and 800 ms were used for cross peak integration and all numerical treatment, as ROESY is prone to artifacts. NOE cross peaks can be observed between protons that spend a significant amount of time close to each other in space. The underlying effect is a direct magnetic dipole−dipole cross-relaxation between the spins during the mixing delay in the pulse sequence, referred to as the mixing time, T_m. The efficiency of the cross relaxation has an inverse r^6 dependence on the interproton distance, a relation that can be used to estimate the distances, r_{ij}, between all protons in a molecule closer to each other than approximately 5 Å, using the cross peak volumes compared to a known distance in the molecule. The qualitative ^{1}H chemical shift observations suggesting Arg-Trp stacking in the case of the *SS/RR* pair but not in the *RS/SR* pair is confirmed by through-space ROE correlations between the two moieties in the former but not in the latter (Figure 10). The difference in Arg-Trp stacking is also supported by the preferred DFT conformers of CAT (Figures 2 and 3). Using the neighboring protons on the rigid indole ring as a reference distance of 2.49 Å, all interproton distances from the *SS/RR* data set were translated to distances using eq 1.

$$r_{ij} = r_{\mathrm{ref}}\left(\frac{a_{\mathrm{ref}}}{a_{ij}}\right)^{1/6} \quad (1)$$

where a is proportional to the cross peak volume and r is the interproton distance. The data set from the *SS/RR* pair was

dx.doi.org/10.1021/jp311151h | J. Phys. Chem. A 2013, 117, 1721−1736

used for numerical treatment of the distances because the qualitatively more folded isomer gives rise to a larger number of detectable contacts. This removes the need to use the absence of a signal as a negative proof, which could in principle happen for more reasons than just being further than 5 Å apart. The extracted distances were compared to the same distances extracted from the three most populated conformations of each enantiomer pair. The calculated Boltzmann distributions were applied as weights and back-calculated volumes were used to average the contribution from each conformer before translating them back to yield distances that are compensated for time averaging of the volumes according to the weighted conformational ensemble.

The recalculated "averaged" distances are found to correlate better to the experimentally derived distances than any of the individual structures in the ensemble does by themselves (Figure S5 in the Supporting Information). For clarity, only interproton distances sensitive to the conformation were selected for distinguishing between the diastereomers. Comparison of the experimentally derived distances from the *SS/RR* data set and the time-averaged theoretical distances reveals a clear correlation for the *SS* ensemble (R^2 = 0.81), whereas there is no correlation in the *RS* ensemble (R^2 = 0.01, Figure 11). The corresponding correlations using the full set of

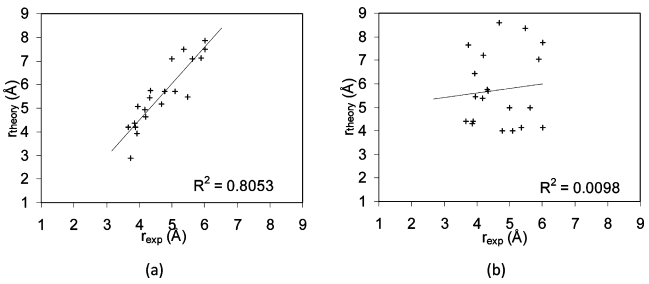

Figure 11. Correlation plots between the experimentally derived interproton distances holding structural information (i.e., distances between protons spanning across the DKP moiety to the opposite side chain) and the theoretical distances compensated for time averaging of the NOE buildup of the ensemble structures. (a) Correlation of the *SS/RR* experimental distances and the *SS*-CAT theoretical distances. (b) Absence of correlation between the *SS/RR* experimental distances and the *RS*-CAT theoretical distances.

interproton distances from the *SS/RR* pair, i.e., also including protons with limited flexibility relative to each other, are R^2 = 0.87 and R^2 = 0.40 for *SS* and *RS*, respectively. The correlation between the experimental and theoretical *SS* data (but not *RS*, Figure 11) allows assignment of *SS*-CAT as belonging to the *SS/RR* enantiomeric pair. For *RS*-CAT, the absence of cross peaks in the NOESY/ROESY spectra of (Figure 10) qualitatively shows that the side-chains are far apart (>5−6 Å), in agreement with the optimized *RS* structures, allowing thus also a tentative assignment of the *RS/SR* isomer.

In proton-rich compounds, such as CAT, the relative stereochemistry of diastereomers is often straightforward to assess with NMR. Which NMR parameter turns out to be most sensitive to the structural differences is highly dependent on the studied molecule. Our analysis shows the convenience of the *J*(C,H) coupling constants and NOE contacts for CAT. However, the clear differences observed in the NOE CAT contacts, where only one isomer pair is folded with a significant Arg-Trp stacking, are rather rare and cannot be generally expected for other flexible molecules.

CONCLUSIONS

The four stereoisomers of the cyclic dipeptide cyclo(Arg-Trp) (CAT) were synthesized, and a combined experimental and computational study was performed to address how the conformational flexibility and the presence of two chiral centers affect the resolution of the absolute configuration by different spectroscopic techniques. The theoretical calculations provided further useful insight into the conformation and the dependence of the spectra on the side-chain orientations and intramolecular interactions. A folded geometry stabilized by intramolecular C−H···π interactions between the DKP ring and the indole group is preferred for all isomers of CAT. For *SS/RR*-CAT but not *SR/RS*-CAT, theoretical and experimental results further support Arg-Trp stacking interactions, resulting in more pronounced molecular folding.

The experimental VCD and ECD spectra could be reliably interpreted on the basis of the calculated conformer populations, but only if solvent and dispersion interactions were properly included in the DFT computations. The two VCD bands at 1298/1299 and 1387/1391 cm^{-1} were identified as the most characteristic peaks allowing the determination of the ACs of the chiral C_1 and C_4 centers of CAT. Reliable ROA spectra could not be recorded for CAT due to sample instabilities. The ECD spectra could be used to determine the configuration of CAT, but only for the second chiral center (C_4), highlighting the advantage of VOA spectroscopies over ECD. NMR analysis provided further information about the folding of CAT, and allowed for the discrimination of *RS/SR* and *SS/RR* isomer pairs on the basis of NOE correlations and *J*(C,H) coupling constants. Combinations of ECD with NMR would also provide a complete AC assignment of CAT. Although this test study was based on isomers with known configuration, our analysis revealed many generally applicable aspects, which can be utilized for further spectroscopic AC determinations of flexible organic compounds.

METHODS

Experimental Details. *IR/VCD Spectra.* Protonated CAT samples were synthesized at the University of Tromsø (Department of Chemistry) using standard procedures.[90] These protonated samples were dissolved in CD_3OD solution (resulting in deuterium exchange at acidic positions). The IR and VCD spectra were measured at the Institute of Chemical Technology (Prague) with an IFS66/S FTIR spectrometer equipped with a PMA 37 VCD/IRRAS module (Bruker). The spectra were measured at a concentration of 0.17 mol/L with a spectral resolution of 4 cm^{-1} using a demountable cuvette A145 with CaF_2 windows and 50 μm optical path length and were baseline corrected by the signal from an identical cuvette filled with solvent. Each spectrum was accumulated for 3−7 h.

ECD Spectra. The ECD spectra were measured using a JASCO J-815 spectrometer at IOCB in Prague. All samples were dissolved in methanol (HPLC grade) at a concentration of 380 μM (0.13 mg/mL). The samples were placed in a quartz cuvette with 1 mm path length and the spectra were recorded in the range of 195−300 at 20 nm/min scanning speed. All the spectra were solvent-corrected and represent an average of three consecutive scans.

dx.doi.org/10.1021/jp311151h | J. Phys. Chem. A 2013, 117, 1721−1736

Raman/ROA Spectra. All samples were dissolved in methanol (HPLC grade) to a concentration of 0.152 M (52 mg/mL) and filled into a quartz cell (3 mm × 3 mm, containing ∼40 μL). Raman and ROA spectra were measured at IOCB in Prague with the Biotools ChiralRAMAN-2X instrument, equipped with an Opus diode-pumped solid-state laser operating at 532 nm. This spectrometer employs backscattering geometry and SCP strategy based on the design by Hug.[91] The laser power was set to 80 mW (which corresponded to ∼40.5 mW reaching the sample), in case of SR the power was 50 mW (at the sample ∼26.4 mW). The samples underwent a partial degradation during the measurements, probably because of the unstable tryptophan residue absorbing close to the laser wavelength. Total acquisition times were 8−32 h. The spectrum of methanol was subtracted from the measured Raman spectra and a baseline correction was made. Note that regions affected by methanol bands (∼1017−1055 and ∼1435−1500 cm^{-1}) are not reliable, and the ROA signal is mostly weak and exhibits a low signal-to-noise ratio.

The VCD, ECD, and ROA spectra were further refined using the fact that enantiomeric pairs give opposite signals.

NMR Experiments. All NMR experiments were recorded on an Agilent (Varian) iNova spectrometer equipped with a cryogenically enhanced inverse HCN probe, operating at 599.934 MHz for ^{1}H and 150.879 MHz for ^{13}C. All experiments were repeated in both CD_3OD and DMSO-d_6 at 298 K, using the residual solvent signal as reference. Assignment of the spectra were recorded using standard pulse sequences in the Chempack 4 package for VnmrJ2.2D, typically gradient-enhanced versions of COSY, ROESY, ^{13}C-HSQC, and ^{13}C-HMBC. The Crisis2 versions of the heteronuclear experiments were used. Through-space NOE correlations were integrated from a series of 2D NOESY spectra at mixing times 200, 300, 500, and 800 ms using Mnova v8.0.0-10524. The volumes were then translated to interproton distances with the two-proton approximation, using the tryptophan ring protons as a reference distance of 2.49 Å. The corresponding distances from the DFT-minimized structures were measured directly in the three most populated structures of each diastereomer and then averaged by back-calculating their corresponding contribution to the observed cross peak (a_{ij}), using the same reference distance and volume as when translating the experimental volumes above. The 800 ms NOESY data were used in the distance calculations. Even though there is limited spin-diffusion taking place at that mixing time, the benefits of higher signal-to-noise ratio of the cross peaks resulting in less integration artifacts makes this preferable over using shorter mixing times (see Figure S6 in the Supporting Information for build-up curves). Long range J(C,H) coupling constants were first calculated from 200 ms constant time HMBC spectra with evolution delays corresponding to between 3 and 20 Hz, modified from the standard adiabatic version of the HMBC pulse sequence by fitting the signal intensity buildup to a sin function.[92] Selected couplings of interest were then reassessed using the recently published double-band selective selEXSIDE pulse sequence using J-scaling factors of 15, 25 and 40×, resulting in digital J resolutions of 0.15−0.39 Hz in the f1 dimension for every coupling.[93] Homonuclear coupling constants were extracted from 1D traces of high-resolution ECOSY, and one-bond heteronuclear couplings were extracted from the adiabatic version of coupled ^{13}C-gHSQC.

Conformational Analysis of Protonated CAT. Five torsion angles (χ_{1-5}, Figure 1a) on the side chain were selected and considered for each stereoisomer; torsion angles χ_{1-4} were systematically varied with 120° angular increments (e.g., −60, +60 and +180°) and χ_5 was determined by the two orientations of the indole group (the phenyl part on the "left" and "right" of the five-membered ring, respectively). Additionally, on the basis of our previous computations on a similar molecule,[29] boat-down and -up DKP conformations (Figure 1b) were considered for the different stereoisomers in the starting search. Using the MCM program,[94] a total of $3^4 \times 2 \times 4 = 648$ structures was generated.

All computations were carried out with the Gaussian 09 package.[95] The B3LYP[96,97] functional and the 6-31++G** basis set were used for geometry optimizations. In addition, the CAM-B3LYP[85−88] and B971[98] functionals were also tested for the reliability of functionals in ECD calculations. Dispersion-corrected[26,27] DFT (DFT-D) was used ($S6$ = 1.00). A previous study[29] confirmed that these methods are very efficient for the modeling of cyclopeptide properties. Optimizations were performed with the IEFPCM model,[99−101] which is well suited for studying charged species.[102] For probing the DKP ring-puckering conformation, the phase and amplitude of the pseudorotation (Q, θ, and P_2) proposed by Haasnoot[82] with a truncated Fourier formalism were employed.

IR Absorption, VCD, Raman, ROA, ECD, and NMR Computations. The IR, VCD, Raman, and ROA spectra of the stereoisomers of CAT were calculated at the B3LYP-D/6-31++G**/IEFPCM(methanol) level of theory. For consistency with the experimental conditions arising from the use of CD_3OD as a solvent (measured for IR and VCD), the calculated IR and VCD signals were adjusted for H−D exchange of the acidic hydrogens (NH, NH_2). The back-scattered Raman and ROA dynamic polarizabilities were generated with an excitation frequency of 532 nm. The Lorentzian band shape with full width at half-maximum of 10 cm^{-1} (at 298 K) was employed to generate the spectral profiles.[83,103] The oscillator strengths and rotational strengths of electronic excitations of all conformers were computed using the TD-DFT method[104−110] at the TD-CAM-B3LYP/6-31++G**/IEFPCM(methanol) level of theory; the rotational strengths were calculated using the velocity representations. Theoretical ECD spectrum of each stable conformer was simulated by using GaussSum 2.2 software[111] (σ = 0.67), where σ refers to the width of the band at 1/e height for the Gaussian curves used to convolute the spectrum. Theoretical NMR parameters (chemical shifts and J(C,H)) coupling constants were computed at the B3LYP/6-31++G**/IEFPCM-(methanol) level of theory on the basis of the dispersion-corrected geometries. All theoretical spectra and NMR parameters were generated by averaging over the conformers using Boltzmann statistics at a temperature of 298 K.

■ ASSOCIATED CONTENT

Supporting Information

Optimized B3LYP geometries without dispersion, experimental and theoretical ROA spectra, comparison of ECD results for CAT and CATM, additional NMR experimental results (selEXSIDE spectra, correlation plots, buildup curves), relative energies and Boltzmann weights, and complete refs 11, 79, and 95. This material is available free of charge via the Internet at http://pubs.acs.org.

AUTHOR INFORMATION

Corresponding Author

*E-mail: bour@uochb.cas.cz (P.B.), kathrin.hopmann@uit.no (K.H.H.).

Notes

The authors declare no competing financial interest.

ACKNOWLEDGMENTS

This work was supported by the Research Council of Norway through a Centre of Excellence grant (Grant No. 179568) and a research grant (Grant No. 191251). P.B. was supported by Academy of Sciences (M200550902), Grant Agency of the Czech Republic (P208/11/0105) and Ministry of Education (LH11033). V.A. was supported by Grant Agency of the Czech Republic (P208/10/0559). A grant of computer time from the Norwegian supercomputing program NOTUR is gratefully acknowledged.

REFERENCES

(1) Corey, R. B. The Crystal Structure of Diketopiperazine. *J. Am. Chem. Soc.* **1938**, *60*, 1598−1604.

(2) Trischman, J. A.; Oeffner, R. E.; Luna, M. G. D.; Kazaoka, M. Competitive Induction and Enhancement of Indole and a Diketopiperazine in Marine Bacteria. *Mar. Biotechnol.* **2004**, *6*, 215−220.

(3) Fukushima, K.; Yazawa, K.; Arai, T. Biological Activities of Albonoursin. *J. Antibiot.* **1973**, *26*, 175−176.

(4) Kanzaki, H.; Imura, D.; Nitoda, T.; Kawazu, K. Enzymatic Conversion of Cyclic Dipeptides to Dehydro Derivatives That Inhibit Cell Division. *J. Biosci. Bioeng.* **2000**, *90*, 86−89.

(5) Nicholson, B.; Lloyd, G. K.; Miller, B. R.; Palladino, M. A.; Kiso, Y.; Hayashi, Y.; Neuteboom, S. T. C. Npi-2358 Is a Tubulin-Depolymerizing Agent: In-Vitro Evidence for Activity as a Tumor Vascular-Disrupting Agent. *Anti-Cancer Drugs.* **2006**, *17*, 25−31.

(6) Brauns, S. C.; Milne, P.; Naudé, R.; Venter, M. V. D. Selected Cyclic Dipeptides Inhibit Cancer Cell Growth and Induce Apoptosis in Ht-29 Colon Cancer Cells. *Anticancer Res.* **2004**, *24*, 1713−1720.

(7) Sinha, S.; Srivastava, R.; Clercq, E. D.; Singh, R. K. Synthesis and Antiviral Properties of Arabino and Ribonucleosides of 1,3-Dideazaadenine, 4-Nitro-1, 3-Dideazaadenine and Diketopiperazine. *Nucleosides, Nucleotides Nucleic Acids* **2004**, *23*, 1815−1824.

(8) Lucietto, F. R.; Milne, P. J.; Kilian, G.; Frost, C. L.; Venter, M. V. D. The Biological Activity of the Histidine-Containing Diketopiperazines Cyclo(His-Ala) and Cyclo(His-Gly). *Peptides* **2006**, *27*, 2706−2714.

(9) Martins, M. B.; Carvalho, I. Diketopiperazines: Biological Activity and Synthesis. *Tetrahedron* **2007**, *63*, 9923−9932.

(10) López-Rodríguez, M. L.; Morcillo, M. J.; Fernández, E.; Porras, E.; Orensanz, L.; Beneytez, M. E.; Manzanares, J.; Fuentes, J. A. Synthesis and Structure−Activity Relationships of a New Model of Arylpiperazines. 5.[1] Study of the Physicochemical Influence of the Pharmacophore on 5-HT_{1A}/α_1-Adrenergic Receptor Affinity: Synthesis of a New Derivative with Mixed 5-HT_{1A}/D_2 Antagonist Properties. *J. Med. Chem.* **2001**, *44*, 186−197.

(11) Wyatta, P. G.; Allenb, M. J.; Borthwicka, A. D.; Daviesa, D. E.; Exalla, A. M.; Hatleya, R. J. D.; Irvinga, W. R.; Livermorea, D. G.; Millera, N. D.; Nerozzia, F.; et al. 2,5-Diketopiperazines as Potent and Selective Oxytocin Antagonists 1: Identification, Stereochemistry and Initial SAR. *Bioorg. Med. Chem. Lett.* **2005**, *15*, 2579−2582.

(12) Kilian, G.; Jamie, H.; Brauns, S. C. A.; Dyason, K.; Milne, P. Biological Activity of Selected Tyrosine-Containing 2, 5-Diketopiperazines. *J. Pharmazie* **2005**, *60*, 305−309.

(13) Bina, X. R.; Bina, J. E. The Cyclic Dipeptide Cyclo(Phe-Pro) Inhibits Cholera Toxin and Toxin-Coregulated Pilus Production in O1 El Tor Vibrio Cholerae. *J. Bacteriol.* **2010**, *192*, 3829−3832.

(14) McCleland, K.; Milne, P. J.; Lucieto, F. R.; Frost, C.; Brauns, S. C.; Venter, M. V. D.; Plessis, J. D.; Dyason, K. An Investigation into the Biological Activity of the Selected Histidine-Containing Diketopiperazines Cyclo(His-Phe) and Cyclo(His-Tyr). *J. Pharm. Pharmacol.* **2004**, *56*, 1143−1153.

(15) Bettens, F. L.; Bettens, R. P. A.; Brown, R. D.; Godfrey, P. D. The Microwave Spectrum, Structure, and Ring-Puckering of the Cyclic Dipeptide Diketopiperazine. *J. Am. Chem. Soc.* **2000**, *122*, 5856−5860.

(16) Brady, G. P.; Sharp, K. A. Energetics of Cyclic Dipeptide Crystal Packing and Solvation. *Biophys. J.* **1997**, *72*, 913−927.

(17) Blancoa, F.; Alkorta, I.; Rozas, I.; Elguero, J. Chiral Recognition in Self-Complexes of Diketopiperazine Derivatives. *J. Phys. Org. Chem.* **2010**, *23*, 1155−1172.

(18) Kapitán, J.; Baumruk, V.; Bouř, P. Demonstration of the Ring Conformation in Polyproline by the Raman Optical Activity. *J. Am. Chem. Soc.* **2006**, *128*, 2438−2443.

(19) Kapitán, J.; Baumruk, V.; Kopecký, V. J.; Pohl, R.; Bouř, P. Proline Zwitterion Dynamics in Solution, Glass, and Crystalline State. *J. Am. Chem. Soc.* **2006**, *128*, 13451−13462.

(20) Andrushchenko, V.; Tsankov, D.; Krasteva, M.; Wieser, H.; Bouř, P. Spectroscopic Detection of DNA Quadruplexes by Vibrational Circular Dichroism. *J. Am. Chem. Soc.* **2011**, *133*, 15055−15064.

(21) Musa, K. A. K.; Eriksson, L. A. Theoretical Assessment of Naphazoline Redoxchemistry and Photochemistry. *J. Phys. Chem. B* **2007**, *111*, 3977−3981.

(22) Li, X.-J.; Zhong, Z.-J.; Wu, H.-Z. DFT and MP2 Investigations of L-Proline and Its Hydrated Complexes. *J. Mol. Model.* **2011**, *17*, 2623−2630.

(23) Ruud, K.; Helgaker, T.; Bouř, P. Gauge-Origin Independent Density-Functional Theory Calculations of Vibrational Raman Optical Activity. *J. Phys. Chem. A* **2002**, *106*, 7448−7455.

(24) Solheim, H.; Kornobis, K.; Ruud, K.; Kozlowski, P. M. Electronically Excited States of Vitamin B12 and Methylcobalamin: Theoretical Analysis of Absorption, Cd, and Mcd Data. *J. Phys. Chem. B* **2011**, *115*, 737−748.

(25) Cohen, A. J.; Mori-Sanchez, P.; Yang, W. Challenges for Density Functional Theory. *Chem. Rev.* **2012**, *112*, 289−320.

(26) Grimme, S. Accurate Description of Van Der Waals Complexes by Density Functional Theory Including Empirical Corrections. *J. Comput. Chem.* **2004**, *25*, 1463−1473.

(27) Grimme, S. Semiempirical GGA-Type Density Functional Constructed with a Long-Range Dispersion Correction. *J. Comput. Chem.* **2006**, *27*, 1787−1799.

(28) Grimme, S.; Antony, J.; Ehrlich, S.; Krieg, H. A Consistent and Accurate Ab Initio Parametrization of Density Functional Dispersion Correction (DFT-D) for the 94 Elements H-Pu. *J. Chem. Phys.* **2010**, *132*, 154104−154119.

(29) Li, X.; Hopmann, K. H.; Hudecová, J.; Stensen, W.; Novotná, J.; Urbanová, M.; Svendsen, J.-S.; Bouř, P.; Ruud, K. Absolute Configuration of a Cyclic Dipeptide Reflected in Vibrational Optical Activity: Ab Initio and Experimental Investigation. *J. Phys. Chem. A* **2012**, *116*, 2554−2563.

(30) Kim, D.; Brédas, J.-L. Triplet Excimer Formation in Platinum-Based Phosphors: A Theoretical Study of the Roles of Pt-Pt Bimetallic Interactions and Interligand Π-Π Interactions. *J. Am. Chem. Soc.* **2009**, *131*, 11371−11380.

(31) Parac, M.; Etinski, M.; Peric, M.; Grimme, S. A Theoretical Investigation of the Geometries and Binding Energies of Molecular Tweezer and Clip Host−Guest Systems. *J. Chem. Theory Comput.* **2005**, *1*, 1110−1118.

(32) Mendham, A. P.; Potter, B. S.; Palmer, R. A.; Dines, T. J.; Mitchell, J. C.; Withnall, R.; Chowdhry, B. Z. Vibrational Spectra and Crystal Structure of the Di-Amino Acid Peptide Cyclo(L-Met-L-Met): Comparison of Experimental Data and DFT Calculations. *J. Raman Spectrosc.* **2010**, *41*, 148−159.

(33) Mendham, A. P.; Palmer, R. A.; Potter, B. S.; Dines, T. J.; Snowden, M. J.; Withnall, R.; Chowdhry, B. Z. Vibrational Spectroscopy and Crystal Structure Analysis of Two Polymorphs of

the Di-Amino Acid Peptide Cyclo(L-Glu-L-Glu). *J. Raman Spectrosc.* **2010**, *41*, 288−302.
(34) Mendham, A. P.; Dines, T. J.; Snowden, M. J.; Withnall, R.; Chowdhry, B. Z. Ir/Raman Spectroscopy and DFT Calculations of Cyclic Di-Amino Acid Peptides. Part III: Comparison of Solid State and Solution Structures of Cyclo(L-Ser-L-Ser). *J. Raman Spectrosc.* **2009**, *40*, 1508−1520.
(35) Mendham, A. P.; Dines, T. J.; Withnall, R.; Mitchell, J. C.; Chowdhry, B. Z. Vibrational Spectroscopic Studies of the Structure of Di-Amino Acid Peptides. Part II: Cyclo(L-Asp-L-Asp) in the Solid State and in Aqueous Solution. *J. Raman Spectrosc.* **2009**, *40*, 1498−1507.
(36) Mendham, A. P.; Dines, T. J.; Snowden, M. J.; Chowdhry, B. Z.; Withnall, R. Vibrational Spectroscopy and DFT Calculations of Di-Amino Acid Cyclic Peptides. Part I: Cyclo(Gly-Gly), Cyclo(L-Ala-L-Ala) and Cyclo(L-Ala-Gly) in the Solid State and in Aqueous Solution. *J. Raman Spectrosc.* **2009**, *40*, 1478−1497.
(37) Bouř, P.; Sychrovský, V.; Maloň, P.; Hanzlíková, J.; Baumruk, V.; Pospíšek, J.; Buděšínský, M. Conformation of the Dipeptide Cyclo(L-Pro-L-Pro) Monitored by the Nuclear Magnetic Resonance and Raman Optical Activity Spectra. Experimental and Ab Initio Computational Study. *J. Phys. Chem. A* **2002**, *106*, 7321−7327.
(38) Kopple, K. D.; Ohnishi, M. Conformations of Cyclic Peptides. II. Side-Chain Conformation and Ring Shape in Cyclic Dipeptides. *J. Am. Chem. Soc.* **1969**, *91*, 962−970.
(39) Fava, G. G.; Belicchi, M. F.; Marchelli, R.; Dossena, A. Synthesis, Crystal Structure and Conformation of the Cyclic Dipeptide Cyclo(-L-Seryl-L-Seryl-). *Acta Crystallogr.* **1981**, *B37*, 625−629.
(40) Hopmann, K. H.; Šebestík, J.; Novotná, J.; Stensen, W.; Urbanová, M.; Svenson, J.; Svendsen, J. S.; Bouř, P.; Ruud, K. Determining the Absolute Configuration of Two Marine Compounds Using Vibrational Chiroptical Spectroscopy. *J. Org. Chem.* **2012**, *77*, 858−869.
(41) Meddour, A.; Berdague, P.; Hedli, A.; Courtieu, J.; Lesot, P. Proton-Decoupled Carbon-13 NMR Spectroscopy in a Lyotropic Chiral Nematic Solvent as an Analytical Tool for the Measurement of the Enantiomeric Excess. *J. Am. Chem. Soc.* **1997**, *119*, 4502−4508.
(42) Fu, G.; Doerksen, R. J.; Xu, P. Assignment of Absolute Configuration of Sulfinyl Dilactones: Optical Rotations and ^{1}H NMR Experiment and DFT Calculations. *J. Mol. Struct.* **2011**, *987*, 166−173.
(43) Wiedemann, S.; Metsala, A.; Nolting, D.; Weinkauf, R. The Dipeptide Cyclic(Glycyltryptophanyl) in the Gas Phase: A Concerted Action of Density Functional Calculations, S0−S1 Two-Photon Ionization, Spectral UV/UV Hole Burning and Laser Photoelectron Spectroscopy. *Phys. Chem. Chem. Phys.* **2004**, *6*, 2641−2649.
(44) Li, Z.; Mukamel, S. First-Principles Simulation of Amide and Aromatic Side Chain Ultraviolet Spectroscopy of a Cyclic Dipeptide. *J. Phys. Chem. A* **2007**, *111*, 11579−11583.
(45) Bowman, R. L.; Kellerman, M.; Johnson, W. C. J. Optical Properties of Cyclic Dimers of Amino Acids: An Experimental and Theoretical Study. *Biopolymers* **1983**, *22*, 1045−1070.
(46) Tamburro, A. M.; Guantieri, V.; Scatturin, A. Conformational Studies on Methionyl-Containing Diketopiperazines. *Int. J. Biol. Macromol.* **1982**, *4*, 126−127.
(47) Nafie, L. A.; Cheng, J. C.; Stephens, P. J. Vibrational Circular Dichroism of 2,2,2-Trifluoro-1-Phenylethanol. *J. Am. Chem. Soc.* **1975**, *97*, 3842−3843.
(48) Stephens, P. J. Theory of Vibrational Circular Dichroism. *J. Phys. Chem. A* **1985**, *89*, 748−752.
(49) Barron, L. D. *Molecular Light Scattering and Optical Activity*, 2nd ed.; Cambridge University Press: Cambridge, U.K., 2004.
(50) Hug, W.; Kint, S.; Bailey, G. F.; Scherer, J. R. Raman Circular Intensity Differential Spectroscopy. Spectra of (2)-a-Pinene and (1)-a-Phenylethylamine. *J. Am. Chem. Soc.* **1975**, *97*, 5589−5590.
(51) Pecul, M.; Ruud, K. Ab Initio Calculation of Vibrational Raman Optical Activity. *Int. J. Quantum Chem.* **2005**, *104*, 816−829.
(52) Ruud, K.; Thorvaldsen, A. J. Theoretical Approaches to the Calculation of Raman Optical Activity Spectra. *Chirality* **2009**, *21*, E54−E67.
(53) Magyarfalvi, G.; Tarczay, G.; Vass, E. Vibrational Circular Dichroism. *Wiley Interdiscip. Rev.: Comput. Mol. Sci.* **2011**, *1*, 403−425.
(54) Aamouche, A.; Stephens, P. J. Conformational Analysis in Solution of a Chiral Bisoxazoline Molecule: Vibrational Circular Dichroism Spectroscopy and Density Functional Theory Study. *Int. J. Spectrosc.* **2011**, *2011*, 905045−11.
(55) Profant, V.; Baumruk, V.; Li, X.; Šafařík, M.; Bouř, P. Tracking of the Polyproline Folding by Density Functional Computations and Raman Optical Activity Spectra. *J. Phys. Chem. B* **2011**, *115*, 15079−15089.
(56) Polyanichko, A.; Wieser, H. Structural Organization of DNA−Protein Complexes of Chromatin Studied by Vibrational and Electronic Circular Dichroism. *Spectroscopy* **2010**, *24*, 239−244.
(57) McColl, I. H.; Blanch, E. W.; Hecht, L.; Barron, L. D. A Study of A-Helix Hydration in Polypeptides, Proteins, and Viruses Using Vibrational Raman Optical Activity. *J. Am. Chem. Soc.* **2004**, *126*, 8181−8188.
(58) Shanmugam, G.; Polavarapu, P. L.; Kendall, A.; Stubbs, G. Structures of Plant Viruses from Vibrational Circular Dichroism. *J. Gen. Virol.* **2005**, *86*, 2371−2377.
(59) Blanch, E. W.; Hecht, L.; Syme, C. D.; Volpetti, V.; Lomonossoff, G. P.; Barron, L. D. Molecular Structures of Viruses from Raman Optical Activity. *J. Gen. Virol.* **2002**, *83*, 2593−2600.
(60) Qiu, F.; Zhang, Y.; Caceres-Cortes, J.; Reily, M. D. Applications of Vibrational Circular Dichroism for Determining Absolute Configuration in Early Drug Discovery. *Am. Lab.* **2010**, *42*, 33−34.
(61) Nieto-Ortega, B.; Casado, J.; Blanch, E. W.; Navarrete, J. T. L.; Quesada, A. R.; Ramirez, F. J. Raman Optical Activity Spectra and Conformational Elucidation of Chiral Drugs. The Case of the Antiangiogenic Aeroplysinin-1. *J. Phys. Chem. A* **2011**, *115*, 2752−2755.
(62) Stephens, P. J.; McCann, D. M.; Devlin, F. J.; A. B. Smith, I. Determination of the Absolute Configurations of Natural Products Via Density Functional Theory Calculations of Optical Rotation, Electronic Circular Dichroism, and Vibrational Circular Dichroism: The Cytotoxic Sesquiterpene Natural Products Quadrone, Suberosenone, Suberosanone, and Suberosenol a Acetate. *J. Nat. Prod.* **2006**, *69*, 1055−1064.
(63) Stephens, P. J.; Pan, J. J.; Devlin, F. J.; Krohn, K.; Kurtan, T. Determination of the Absolute Configurations of Natural Products Via Density Functional Theory Calculations of Vibrational Circular Dichroism, Electronic Circular Dichroism, and Ptical Rotation: The Iridoids Plumericin and Isoplumericin. *J. Org. Chem.* **2007**, *72*, 3521−3536.
(64) Polavarapu, P. L.; Donahue, E. A.; Shanmugam, G.; Scalmani, G.; Hawkins, E. K.; Rizzo, C.; Ibnusaud, I.; Thomas, G.; Habel, D.; Sebastian, D. A Single Chiroptical Spectroscopic Method May Not Be Able to Establish the Absolute Configurations of Diastereomers: Dimethylesters of Hibiscus and Garcinia Acids. *J. Phys. Chem. A* **2011**, *115*, 5665−5673.
(65) Srebro, M.; Govind, N.; Jong, W. A. d.; Autschbach, J. Optical Rotation Calculated with Time-Dependent Density Functional Theory: The Or45 Benchmark. *J. Phys. Chem. A* **2011**, *115*, 10930−10949.
(66) Crawford, T. D.; Tam, M. C.; Abrams, M. L. The Current State of Ab Initio Calculations of Optical Rotation and Electronic Circular Dichroism Spectra. *J. Phys. Chem. A* **2007**, *111*, 12057−12068.
(67) Zhao, S.-D.; Shen, L.; Luo, D.-Q.; Zhu, H.-J. Progression of Absolute Configuration Determination in Natural Product Chemistry Using Optical Rotation (Dispersion), Matrix Determinant and Electronic Circular Dichroism Methods. *Curr. Org. Chem.* **2011**, *15*, 1843−1862.
(68) Stephens, P. J.; McCann, D. M.; Devlin, J.; Cheeseman, J. R.; Frisch, M. J. Determination of the Absolute Configuration of [3_2](1,4)Barrelenophanedicarbonitrile Using Concerted Time-Dependent Density Functional Theory Calculations of Optical Rotation and Electronic Circular Dichroism. *J. Am. Chem. Soc.* **2004**, *126*, 7514−7521.

(69) Jiemchooroj, A.; Norman, P. Electronic Circular Dichroism Spectra from the Complex Polarization Propagator. *J. Chem. Phys.* **2007**, *126*, 134102−134107.
(70) Mukhopadhyay, P.; Zuber, G.; Goldsmith, M.-R.; Wipf, P.; Beratan, D. N. Solvent Effect on Optical Rotation: A Case Study of Methyloxirane in Water. *ChemPhysChem* **2006**, *7*, 2483−2486.
(71) Polavarapu, P. L. Why Is It Important to Simultaneously Use More Than One Chiroptical Spectroscopic Method for Determining the Structures of Chiral Molecules? *Chirality* **2007**, *20*, 605−759.
(72) Hallwass, F.; Schmidt, M.; Sun, H.; Mazur, A.; Kummerlöwe, G.; Luy, B.; Navarro-Vázquez, A.; Griesinger, C.; Reinscheid, U. M. Residual Chemical Shift Anisotropy (Rcsa): A Tool for the Analysis of the Configuration of Small Molecules. *Angew. Chem., Int. Ed.* **2011**, *50*, 9487−9490.
(73) Gil, R. R.; Gayathri, C.; Tsarevsky, N. V.; Matyjaszewski, K. Stretched Poly(Methyl Methacrylate) Gel Aligns Small Organic Molecules in Chloroform. Stereochemical Analysis and Diastereotopic Proton NMR Assignment in Ludartin Using Residual Dipolar Couplings and 3j Coupling Constant Analysis. *J. Org. Chem.* **2008**, *73*, 840−848.
(74) Freudenberger, J. C.; Knör, S.; Kobzar, K.; Heckmann, D.; Paululat, T.; Kessler, H.; Luy, B. Stretched Poly(Vinyl Acetate) Gels as NMR Alignment Media for the Measurement of Residual Dipolar Couplings in Polar Organic Solvents. *Angew. Chem., Int. Ed.* **2005**, *44*, 423−426.
(75) Thiele, C. M. Simultaneous Assignment of All Diastereotopic Protons in Strychnine Using RDCs: PELG as Alignment Medium for Organic Molecules. *J. Org. Chem.* **2004**, *69*, 7403−7413.
(76) Wenzel, T. J.; Chisholm, C. D. Using NMR Spectroscopic Methods to Determine Enantiomeric Purity and Assign Absolute Stereochemistry. *Prog. Nucl. Magn. Reson. Spectrosc.* **2011**, *59*, 1−63.
(77) Marathias, V. M.; Tawa, G. J.; Goljer, I.; Bach, A. C. Stereochemical Identification of (R)- and (S)-Ibuprofen Using Residual Dipolar Couplings, NMR, and Modeling. *Chirality* **2007**, *19*, 741−750.
(78) Nath, N.; Suryaprakash, N. Spin-Selective Correlation Experiment for Measurement of Long-Range J Couplings and for Assignment of (R/S) Enantiomers from the Residual Dipolar Couplings and DFT. *J. Phys. Chem. B* **2011**, *115*, 6868−6875.
(79) Berger, R.; Courtieu, J.; Gil, R. R.; Griesinger, C.; Köck, M.; Lesot, P.; Luy, B.; Merlet, D.; Navarro-Vázquez, A.; Reggelin, M.; et al. Is Enantiomer Assignment Possible by NMR Spectroscopy Using Residual Dipolar Couplings from Chiral Nonracemic Alignment Media?—a Critical Assessment. *Angew. Chem., Int. Ed.* **2012**, *51*, 8388−8391.
(80) Kopple, K. D.; Marr, D. H. Conformations of Cyclic Peptides. Folding of Cyclic Dipeptides Containing an Aromatic Side Chain. *J. Am. Chem. Soc.* **1967**, *89*, 6193−6200.
(81) Brienne, M.-J.; Gabard, J.; Leclercq, M.; Lehn, J.-M.; Cesario, M.; Pascard, C.; Chevé, M.; Dutruc-Rosset, G. Chirality Directed Self-Assembly. Resolution of 2,5-Diazabicyclo[2.2.2]Octane-3,6-Dione and Crystal Structures of Its Racemic and (−) Enantiomeric Forms. *Tetrahedron Lett.* **1994**, *35*, 8157−8160.
(82) Haasnoot, C. The Conformation of Six-Membered Rings Described by Puckering Coordinates Derived from Endocyclic Torsion Angles. *J. Am. Chem. Soc.* **1992**, *114*, 882−887.
(83) Yamamoto, S.; Straka, M.; Watarai, H.; Bouř, P. Formation and Structure of the Potassium Complex of Valinomycin in Solution Studied by Raman Optical Activity Spectroscopy. *Phys. Chem. Chem. Phys.* **2010**, *12*, 11021−11032.
(84) Hudecová, J.; Horníček, J.; Buděšínský, M.; Šebestík, J.; Šafařík, M.; Zhang, G.; Keiderling, T. A.; Bouř, P. Three Types of Induced Tryptophan Optical Activity Compared in Model Dipeptides: Theory and Experiment. *ChemPhysChem* **2012**, *13*, 2748−2760.
(85) Kobayashi, R.; Amos, R. D. The Application of CAM-B3LYP to the Charge-Transfer Band Problem of the Zincbacteriochlorin−Bacteriochlorin Complex. *Chem. Phys. Lett.* **2006**, *420*, 106−109.
(86) Yanai, T.; Harrison, R. J.; Handy, N. C. Multiresolution Quantum Chemistry in Multiwavelet Bases: Time-Dependent Density Functional Theory with Asymptotically Corrected Potentials in Local Density and Generalized Gradient Approximations. *Mol. Phys.* **2005**, *103*, 413−424.
(87) Peach, M. J. G.; Helgaker, T.; Sałek, P.; Keal, T. W.; Lutnæs, O. B.; Tozer, D. J.; Handy, N. C. Assessment of a Coulomb-Attenuated Exchange−Correlation Energy Functional. *Phys. Chem. Chem. Phys.* **2006**, *8*, 558−562.
(88) Vydrov, O. A.; Scuseria, G. E. Assessment of a Long-Range Corrected Hybrid Functional. *J. Chem. Phys.* **2006**, *125*, 234109−234109.
(89) Yanaia, T.; Tew, D. P.; Handy, N. C. A New Hybrid Exchange−Correlation Functional Using the Coulomb-Attenuating Method (CAM-B3LYP). *Chem. Phys. Lett.* **2004**, *393*, 51−57.
(90) Johnson, A.-L.; Bergman, J.; Sjogren, M.; Bohlin, L. Synthesis of Barettin. *Tetrahedron* **2004**, *60*, 961−965.
(91) Hug, W.; Hangartner, G. A Novel High-Throughput Raman Spectrometer for Polarization Difference Measurements. *J. Raman Spectrosc.* **1999**, *30*, 841−852.
(92) Willker, W.; Leibfritz, D. Determination of Heteronuclear Long-Range H,X Coupling Constants from Gradient-Selected Hmbc Spectra. *Magn. Reson. Chem.* **1995**, *33*, 632−638.
(93) Butts, C. P.; Heise, B.; Tatolo, G. Selexside: Fast and Easy Measurement of Multiple-Bond 1H,13C Coupling Constants for Stereochemical Analysis. *Org. Lett.* **2012**, *14*, 3256−3259.
(94) Bouř, P.; Maloň, P. The MCM Program. The MCM program 1995−2009, Academy of Sciences, Prague.
(95) Frisch, M. J.; Trucks, G. W.; Schlegel, H. B.; Scuseria, G. E.; Robb, M. A.; Cheeseman, J. R.; Scalmani, G.; Barone, V.; Mennucci, B.; Petersson, G. A.; et al.; *Gaussian 09*, Revision B.01: Gaussian, Inc.: Wallingford, CT, 2009.
(96) Becke, A. D. Density-Functional Exchange-Energy Approximation with Correct Asymptotic Behavior. *Phys. Rev. A* **1988**, *38*, 3098−3100.
(97) Lee, C.; Yang, W.; Parr, R. G. Development of the Colle-Salvetti Correlation-Energy Formula into a Functional of the Electron Density. *Phys. Rev. B* **1988**, *37*, 785−789.
(98) Hamprecht, F. A.; Cohen, A. J.; Tozer, D. J.; Handy, N. C. Development and Assessment of New Exchange-Correlation Functionals. *J. Chem. Phys.* **1998**, *109*, 6264−6268.
(99) Cances, E.; Mennucci, B.; Tomasi, J. A New Integral Equation Formalism for the Polarizable Continuum Model: Theoretical Background and Applications to Isotropic and Anisotropic Dielectrics. *J. Chem. Phys.* **1997**, *107*, 3032−3010.
(100) Tomasi, J.; Persico, M. Molecular Interactions in Solution: An Overview of Methods Based on Continuous Distributions of the Solvent. *Chem. Rev.* **1994**, *94*, 2027−2094.
(101) Tomasi, J.; Mennucci, B.; Cammi, R. Quantum Mechanical Continuum Solvation Models. *Chem. Rev.* **2005**, *105*, 2999−3094.
(102) Biot, C.; Buisine, E.; Rooman, M. Free-Energy Calculations of Protein−Ligand Cation−Π and Amino−Π Interactions: From Vacuum to Proteinlike Environments. *J. Am. Chem. Soc.* **2003**, *125*, 13988−13994.
(103) Buděšinský, M.; Daněček, P.; Bednárová, L.; Kapitán, J.; Baumruk, V.; Bouř, P. Comparison of Quantitative Conformer Analyses by Nuclear Magnetic Resonance and Raman Optical Activity Spectra for Model Dipeptides. *J. Phys. Chem. A* **2008**, *112*, 8633−8640.
(104) Bauernschmitt, R.; Ahlrichs, R. Treatment of electronic excitations within the adiabatic approximation of time dependent density functional theory. *Chem. Phys. Lett.* **1996**, *256*, 454.
(105) Casida, M. E.; Jamorski, C.; Casida, K. C.; Salahub, D. R. Molecular Excitation Energies to High-Lying Bound States from Time-Dependent Density-Functional Response Theory: Characterization and Correction of the Time-Dependent Local Density Approximation Ionization Threshold. *J. Chem. Phys.* **1998**, *108*, 4439−4449.
(106) Stratmann, R. E.; Scuseria, G. E.; Frisch, M. J. An Efficient Implementation of Time-Dependent Density-Functional Theory for the Calculation of Excitation Energies of Large Molecules. *J. Chem. Phys.* **1998**, *109*, 8218−8224.

(107) Van Caillie, C.; Amos, R. D. Geometric Derivatives of Excitation Energies Using SCF and DFT. *Chem. Phys. Lett.* **1999**, *308*, 249−255.
(108) Van Caillie, C.; Amos, R. D. Geometric Derivatives of Density Functional Theory Excitation Energies Using Gradient-Corrected Functionals. *Chem. Phys. Lett.* **2000**, *317*, 159−164.
(109) Furche, F.; Ahlrichs, R. Adiabatic Time-Dependent Density Functional Methods for Excited State Properties. *J. Chem. Phys.* **2002**, *117*, 7433−7447.
(110) Scalmani, G.; Frisch, M. J.; Mennucci, B.; Tomasi, J.; Cammi, R.; Barone, V. Geometries and properties of excited states in the gas phase and in solution: Theory and application of a time-dependent density functional theory polarizable continuum model. *J. Chem. Phys.* **2006**, *124*, 094107−094121.
(111) O'Boyle, N. M.; Tenderholt, A. L.; Langner, K. M. Cclib: A Library for Package-Independent Computational Chemistry Algorithms. *J. Comput. Chem.* **2008**, *29*, 839−845.